DOI: 10.15587/978-617-8360-09-2.CH1

Bogdana Gayvas, Bogdan Markovych, Anatolii Dmytruk, Veronika Dmytruk

CHAPTER 1

CHAPTER 1

CONVECTIVE DRYING OF WOOD OF CYLINDRICAL SHAPE

ABSTRACT

In this Chapter, the mathematical nonstationary and quasi-stationary models of the heat and moisture transfer in convective drying of a long wooden beam with a circular cross-section of the radius R ($0 \le r \le R$) are constructed, taking into account the moving boundary of the moisture evaporation zone under the action of the convective-thermal unsteady flow of the drying agent, as well as the calculation schemes for the implementation of these models into practice. Numerical experiments are carried out. The regularities of distribution of temperature and moisture in a capillary-porous body of a cylindrical shape at an arbitrary moment of drying depending on the coordinate of the phase transition, thermophysical characteristics of the material, and parameters of the drying agent have been established.

KEYWORDS

Mathematical model, initial boundary value problem, heat and mass transfer, convection, diffusion, Stefan's problem, Kontorovich-Lebedev transform, Pochhammer's polynomials, Green's function, Steklov's theorem, Poiseuille's equation, capillary-porous material, phase transition, cylindrical shape.

Drying is the process of removing moisture from the body, which changes the structural-mechanical, technological and biological properties of the material, caused by the change in bonding forms of moisture with the material [1, 2]. When moisture is removed, capillary-porous bodies become brittle, slightly compressible and can be turned into powder; colloidal bodies significantly change their size with changing moisture content, but retain plasticity or elastic properties; capillary-porous colloidal bodies have a capillary-porous structure, with capillary walls having the properties of limitedly swollen colloidal bodies (skin, tissue, wood) [3–5].

Convective-heat drying is classified into subtypes: steam-air, gas, steam, moisture and others [6]. The uniformity of drying materials in drying plants is achieved by the drying agent circulation. The drying agent circulation with velocity υ can be natural and forced, unilateral and reversible. It is carried out by fans in a chamber or through ejector nozzles [6]. The drying agent is characterized additionally by humidity $\phi = \frac{\gamma_v}{\gamma_n}$ and temperature t. Here, γ_v is the density of vapor, and γ_n is the density of saturated vapor. Parameters t, φ, υ define the drying mode [6].

The change of local moisture content U and local temperature t in a capillary-porous body with time depends on the relationship between the mechanism of moisture and heat transfer inside the wet material as well as the mass and heat exchange of the body surface with the drying agent [7–9].

In drying plants, the regime changes with time. A rigorous analysis of drying kinetics is complex. Increasing temperature intensifies the drying process [10, 11]. Increasing the moisture content of the drying agent reduces the intensity and critical moisture content [12, 13]. Increasing the velocity of the drying agent leads to higher drying intensity at the beginning of the process and has much less effect at the end [14].

The whole process of drying porous materials can be divided into three stages [6]:

1. Disordered irregular regime at the beginning of the process. The initial distribution of temperature and moisture in the body is important here.

2. From some time on, the body enters a regular heating regime, when the initial distribution no longer has an effect. Body heating is described by a simple exponent.

3. The final stage of heating corresponds to the stationary state, at which the temperature is equal to the ambient temperature at all points of the body.

During the drying process, three characteristic zones can be formed in the body: the outer gas zone, where all the pores are dried; the middle two-phase zone, where the dried pores and the pores filled with moisture; and the inner moisture zone, where all the pores are filled with moisture. The two-phase zone emerges due to the release of moisture through evaporation, and on the other hand, through the flow of moisture by the action of capillary forces from wide moisture pores into narrow dried pores and recondensation of moisture. In the elementary physical volume of the two-phase zone, the moisture phase may exist in the form of a connected network of wet pores and in the form of unconnected inclusions, blocked by gas from all sides. Their fates depend on the specific moisture content. In the process of evaporation with a decrease in specific moisture content, redistribution and fragmentation of the cohesive system occur. Upon reaching a critical moisture content, the bonds are completely broken. The capillary inflow is possible only through the connected moisture network. For moisture contents less than critical, the transfer through the moisture phase is impossible. The cohesive system of moisture pores is also heterogeneous due to one-side open pores [4]. The dimension of these zones depends on the pore radius distribution function, which characterizes the structure of the porous body. During evaporation, the boundaries of the zones move into the middle of the body.

Forms of moisture bonding with the material. The velocity of moisture movement inside the material depends on the form of its connection with the material. The main forms of moisture connection with the body are adsorption and capillary bonds [15]. The amount of adsorption-bound and microcapillary moisture depends on the temperature and pressure in the environment. This moisture is called hygroscopic moisture. Changes in material dimensions (shrinkage-soaking) are linked to the change in the amount of hygroscopic moisture. Bound moisture is uniform and depends on the structure of the surface interacting with it. There arises a density gradient in the layer thickness of the water bound to the body surface. Capillary forces and gravity do not occur in this bound water. The evaporation heat of bound water is higher than the one of free water by the energy amount of adsorption water bounding with the surface of $E \approx 280$ cal/g [15].

In the macrocapillaries of a capillary-porous body, the laminar flow satisfies Poiseuille's equation $j = \frac{\rho^2}{8\nu}\frac{P_1 - P_2}{l}$, with P_1, P_2 as the pressure at the ends of the capillary of length l. Poiseuille'e quation and Fick's law of diffusion are not satisfied in microcapillaries, with $j = \frac{8}{3}\sqrt{\frac{\mu}{2\pi RT}}\frac{\varepsilon}{l}\left(\frac{P_2}{\sqrt{T_2}} - \frac{P_1}{\sqrt{T_1}}\right)$ being the flow [16], where μ is the dynamic viscosity, ε is a constant for a capillary-porous body, it is called the coefficient of the molecular gas flow. The heat conduction coefficient for gas in microcapillaries is defined as $\lambda = 2\varepsilon c_\upsilon\sqrt{\frac{\mu}{3RT}}\rho$, where c_υ is the specific heat capacity of gas for the constant volume and ρ is the capillary radius [16].

The forms of moisture bonding with the material play a major role in the mechanism of heat and moisture transfer inside the body.

The main mechanisms of moisture transfer in the porous medium are [17]:

– diffusion of vapor-air mixture in the gas zone by the action of density difference in the direction opposite to the gradient and recondensation by the action of partial pressure gradient of vapor over menisci of different curvature;

– thermal diffusion of vapor in the direction of heat flow from areas with higher temperature to areas with lower temperature;

– convective transfer of vapor and moisture by the action of external pressure drop;

– capillary movement of moisture in the pores that depends on the structure of the porous medium, i.e. the capillary inleakage from wide to narrow pores due to the difference in capillary pressure;

– moisture film transfer by the action of gradients of the wedge and capillary pressures.

Experimental studies of these transfer mechanisms carried out on real and model systems indicate the decisive effect of capillary and surface forces on the mass transfer process and drying intensity. These forces regulate the mutual distribution of phases in the pore space and determine the conditions of transfer, causing the mechanisms of transfer.

The amount of adsorption-bound and microcapillary moisture depends on the temperature and vapor pressure in the environment. The relationship between moisture and the body is characterized by the differential and integral curves of pore radius distribution.

The area under the differential curve on its arbitrary part provides the moisture volume (saturation) within the range of capillary radii change. The curves of pore distribution by radii show a wide variation in the size of voids in the body pores.

To determine the rational drying regime, the choice of which depends on technological changes in the drying process, it is important to study the regularities of moisture transfer for the purpose of its control. One of the possible ways to control the moisture transfer mechanism is by affecting the processes of diffusion and thermal diffusion.

The moisture movement by the action of temperature (heat and moisture conduction) includes the following phenomena [1, 3–5, 10, 17]:

1. Molecular diffusion of moisture in the form of molecular vapor flow, which occurs due to different velocities of molecules of heated and cold material layers.

2. Capillary conduction caused by the change in capillary potential, which depends on the surface tension, decreasing with rising temperature. Since the capillary pressure over the concave meniscus is negative, the decrease in pressure increases the suction force, resulting in moisture leaving the heated body to colder layers in the form of liquid.

3. The movement of fluid in a porous body in the direction of heat flow is caused by trapped air. When the material is heated, the pressure of the trapped air increases, and the air bubbles expand. As a result, the liquid in the capillary pore is pushed in the direction of heat flow.

Heat moisture conduction is the reason for the movement of moisture in the direction of heat flow. During convective drying, a temperature gradient opposite to the moisture gradient is created, which prevents the movement of moisture from the bulk to the surface of the material. The flow of moisture directed to the surface of the material is reduced by the value of the flow of moisture due to thermal diffusion. The temperature gradient is an obstacle to the movement of moisture from the central layers to the surface. With a constant intensity of drying, conditions are created that help the evaporation of moisture inside the material. Thermal diffusion reduces the moisture gradient and reduces the speed of movement of liquid moisture and the amount of water-soluble substances on the surface of the material. With a change in the value and direction of the temperature gradient, the conditions for the movement of moisture and substances dissolved in it change. This leads to a change in the physical and chemical properties of the material [3–5].

1.1 CONVECTIVE DRYING OF WOOD OF CYLINDRICAL SHAPE: NONSTATIONARY CASE

One of the important areas of modern mathematical modeling is the construction of adequate mathematical models for the description of the technological processes of drying capillary-porous materials. Such models, as a rule, are based on the thermodynamics of irreversible processes and must take into account the peculiarities of the kinetics of internal transformations, in particular, phase transitions. The problems of mathematical physics based on them also require the development of appropriate analytical and numerical methods for their solution.

Drying of wood includes taking into account the heat-mass exchange between the wood surface and wet air and the internal heat and moisture exchange in the material [18]. The relationship between the distribution of moisture content and temperature fields depends on the geometric dimensions of the material to be dried. In this chapter, the mathematical nonlinear and linear models of the moisture transfer in drying of a long wooden beam with a circular cross-section of the radius R ($0 \le r \le R$) is constructed, taking into account the moving boundary of the moisture evaporation zone under the action of the convective-thermal unsteady flow of the drying agent as well as the calculation schemes for the implementation of these models into practice. Numerical experiments are carried out. The regularities of distribution of temperature and moisture in a capillary-porous body of a cylindrical shape at an arbitrary moment of drying depending on the coordinate of the phase transition, thermophysical characteristics of the material, and parameters of the drying agent have been established.

When developing the models, it was taken into account that wood shrinkage along the fibers is negligibly small (0.1–0.3 %). The cross-section shrinkage is from 2 to 10 % [6].

Since the length of the considered cylindrical beam is much greater than the dimensions of its cross-section, and the coefficient of moisture conductivity along the fibers is much larger than that coefficient across the fibers, and due to the great complexity of the structure of the wood material, a plane averaged thermal conductivity problem is considered. As a tool for describing thermal conductivity, differential equations were used to model non-stationary processes [19]. The method of integral transformations was used to find solutions [20].

To simplify the models, it is assumed that the gas phase is water vapor, which is an ideal gas.

The aim of this work is the determination of optimal wood drying parameters, at which energy consumption will be minimal.

Problem formulation. Let's consider a cylinder with a radius R ($0 \le r \le R$) shown in **Fig. 1.1**. Given the symmetry of the boundary conditions of this problem, it is possible to introduce a polar coordinate system (r, φ), the polar axis of which is directed along the axis of the cylinder. The cylinder is under the action of convective-thermal non-stationary flow of the drying steam-air agent of the velocity υ. It is possible to assume that the drying agent regime is three-stage, non-stationary, and includes heating, keeping, and cooling.

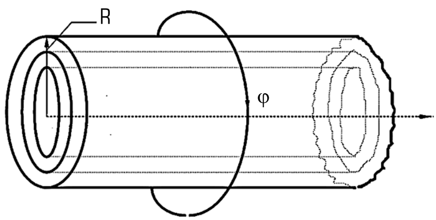

Fig. 1.1 Schematic representation of the wooden cylindrical beam

The control parameter in this process is the temperature of the drying agent T_a. In convective drying, the heat supplied by the gas is used to evaporate the liquid, heat the material, and overcome the energy of moisture bonds with the material. It is possible to assume that the moisture in the dried area is removed and in the rest of the volume it is preserved, known and its density is ρ_L. The moisture content W retained in the body is calculated by the formula:

$$W = \rho_L \left(\frac{V - V_m}{V} \right),$$

where V is the body volume; V_m is the volume of the dried area. Note that when hot air contacts with moisture particles, the latter break down into steam and smaller liquid particles.

The process of heat conduction in the body is described by the equation:

$$\left[\Pi \left(C_v \rho_v + C_a \rho_a \right) + \left(1 - \Pi \right) C_s \rho_s \right] \frac{\partial T}{\partial \tau} + \gamma_1^2 T =$$
$$= \lambda \left[r^2 \frac{d^2 T}{dr^2} + \left(2\alpha + 1 \right) r \frac{dT}{dr} + \left(\alpha^2 - \lambda^2 r^2 \right) T \right], \ \left(2\alpha + 1 > 0 \right). \tag{1.1}$$

where τ is time; r is the radius of running point $(0 \le r \le R)$; γ_1^2 is the particle decomposition coefficient.

Equation (1.1), using the Bessel differential operator, takes the form:

$$B_\alpha \left[T \right] = \left[r^2 \frac{d^2 T}{dr^2} + \left(2\alpha + 1 \right) r \frac{dT}{dr} + \left(\alpha^2 - \lambda^2 r^2 \right) T \right],$$

for the given volumetric heat capacity c_ρ and averaged thermal conductivity λ in the quasi-homogeneous approximation, which can be used in wood drying problems with acceptable temperature gradients, has the form [20]:

$$\frac{\partial T}{\partial \tau} + \gamma^2 T = a^2 B_\alpha \left[T, r \right], \ \gamma^2 = \frac{\gamma_1^2}{c_\rho}, \ \alpha > 0, \tag{1.2}$$

where $a^2 = \dfrac{\lambda}{\left[\Pi (C_v \rho_v + C_a \rho_a) + \left(1 - \Pi \right) C_s \rho_s \right]}$ is the averaged thermal diffusivity coefficient.

Let's construct the solution of Equation (1.2) under the following boundary conditions:

$$T\left(\tau, r \right) \big|_{\tau = 0} = g\left(r \right), \ r \in \left(0, R \right), \tag{1.3}$$

$$\lim \big|_{r \to 0} \frac{\partial}{\partial r} \left(r^\alpha T \right) = 0, \ \left(\alpha_{11}^1 \frac{\partial}{\partial r} + \beta_{11}^1 \right) T \big|_{r \to R} = T_a\left(\tau \right), \tag{1.4}$$

where T_a is the temperature of the drying agent; γ^2 is responsible for the multiplication of particles of the steam-air mixture (averaged coefficient of decomposition) in the porous material under the action of the drying agent; indices v, a, s indicate the components of steam, air, and skeleton, respectively; Π, C_v, C_a, C_s, ρ_v, ρ_a, ρ_s are porosity, heat capacity, and density of steam, air, and skeleton, respectively; λ is the averaged coefficient of thermal conductivity; α_{11}^1, β_{11}^1 are coefficients of thermal conductivity and heat transfer on the outer surface of the cylinder.

The temperature of the drying agent $T_a(\tau)$ is as follows:

$$T_a(\tau)=\begin{cases} T_0+\dfrac{T_{\max}-T_0}{\tau_1}\tau,\ 0\le\tau\le\tau_1; \\ T_{\max},\ \tau_1\le\tau\le\tau_2; \\ \dfrac{T_{\max}\tau_3-T_1\tau_2}{\tau_3-\tau_2}-\dfrac{T_{\max}-T_1}{\tau_3-\tau_2}\tau,\ \tau_2\le\tau\le\tau_3. \end{cases} \tag{1.5}$$

The scheme of $T_a(\tau)$ behavior is shown in **Fig. 1.2**.

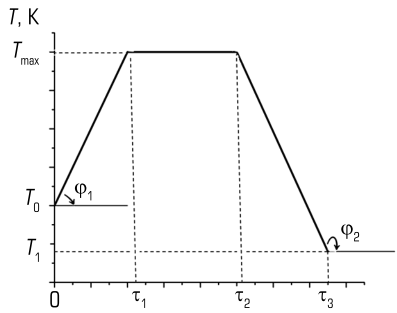

Fig. 1.2 Control function $T_a(\tau)$

Here T_0 is the initial temperature of the drying agent; cooling is carried out to some equilibrium temperature.

It is possible to expand this function into a trigonometric Fourier series with respect to cosines:

$$T_a(\tau)=\alpha_0+\sum_{n=1}^{\infty}\alpha_n\cos\frac{n\pi}{\tau_3}\tau,\ \nu_n^2=\frac{n\pi}{\tau_3}.$$

$$\alpha_0=\frac{2}{\tau_3}\left[T_{\max}\left(-\frac{\tau_1}{2}+\frac{\tau_2}{2}+\frac{\tau_3}{2}\right)+T_0\frac{\tau_1}{2}+T_1\left(-\frac{\tau_2}{2}+\frac{\tau_3}{2}\right)\right],$$

$$\alpha_n = \frac{2}{\tau_3}\left[\frac{\left(T_{\max} - T_0\right)}{\tau_1 \nu_n^4}\left(\cos\nu_n^2\tau_1 - 1\right) + \frac{T_{\max}}{\nu_n^2}(\sin\nu_n^2\tau_2 - \sin\nu_n^2\tau_1)\right] +$$

$$+\frac{2}{\tau_3}\left\{-\frac{T_{\max}\tau_3 - T_1\tau_2}{\tau_3 - \tau_2}\frac{\tau_2}{n\pi}\sin\nu_n^2\tau_2 - \frac{T_{\max} - T_1}{\tau_3 - \tau_2}\left(\frac{1}{\nu_n}\right)^4\left[\left(-1\right)^n - \cos\nu_n^2\tau_2 - \frac{n\pi\tau_2}{\tau_3}\sin\nu_n^2\tau_2\right]\right\}.$$

Let $T^*(p,r)$ be the image of the Laplace transform of the temperature $T(\tau,r)$:

$$L\left[T\left(\tau,r\right)\right] = \int_0^\infty T\left(\tau,r\right)e^{-p\tau}d\tau = T^*\left(p,r\right).$$

Then, in accordance with the problem (1.1)–(1.4), it is possible to obtain the following boundary value problem with respect to the function $T^*(p,r)$:

$$\left(B_{\nu,\alpha} - \lambda^2\right)T^* = \frac{d^2T^*}{dr^2} + \frac{2\alpha+1}{r}\frac{dT^*}{dr} - \left(\lambda^2 + \frac{\nu^2 - \alpha^2}{r^2}\right)T^* = -\tilde{g}\left(r\right), \tag{1.6}$$

$$\lim\Big|_{r\to 0}\frac{\partial}{\partial r}\left(r^{\alpha-\nu}T^*\left(p,r\right)\right) = 0,\ \left(\alpha_{11}^1\frac{d}{dr} + \beta_{11}^1\right)T^*\Big|_{r=R} = T_a^*\left(p\right), \tag{1.7}$$

$$\tilde{g}\left(r\right) = a^{-2}r^{-2}g\left(r\right),\ \nu^2 = a^{-2}\left(p+\gamma^2\right),\ p = \sigma + i\tau,\ i^2 = -1.$$

Let's fix $\operatorname{Re}\nu = \operatorname{Re}\left[a^{-1}\left(p+\gamma^2\right)^{1/2}\right] > 0.$ Construct a Cauchy function for equation (1.6) to satisfy homogeneous boundary conditions. A fundamental function $\varepsilon_\alpha^*(p,r,\rho)$ satisfying the homogeneous equation corresponding to equation (1.6) and the homogeneous conditions corresponding to the conditions (1.7) is the Cauchy function. The solution of equation (1.6) satisfying the homogeneous conditions corresponding to the conditions (1.7), has the form:

$$T^*\left(p,r\right) = \int_0^R \varepsilon_\alpha^*\left(p,r,\rho\right)\tilde{g}\left(\rho\right)\rho^{2\alpha+1}d\rho,$$

where $\varepsilon_\alpha^*(p,r,\rho)$ is a fundamental function of the boundary value problem (1.6), (1.7) with the following properties:

– the function $\varepsilon_\alpha^*(p,r,\rho)$ satisfies the homogeneous equation corresponding to equation (1.6) and the following boundary conditions [20]:

$$\lim\Big|_{r\to 0}\frac{\partial}{\partial r}\left(r^{\alpha-\nu}\varepsilon^*\right)=0,\ \left(\alpha_{1_1}^1\frac{d}{dr}+\beta_{1_1}^1\right)\varepsilon^*\Big|_{r=R}=0.$$

With this, $\varepsilon_\alpha^*(p,r,\rho)\big|_{r=\rho+0}-\varepsilon_\alpha^*(p,r,\rho)\big|_{r=\rho-0}=0.$

The following holds $d/dr\varepsilon_\alpha^*(p,r,\rho)\big|_{r=\rho+0}-d/dr\varepsilon_\alpha^*(p,r,\rho)\big|_{r=\rho-0}=\rho^{-(2\alpha+1)}$.

Let's put:

$$\varepsilon_\alpha^*(p,r,\rho)=\begin{cases}A_1 I_{\nu,\alpha}(\lambda\rho),\ 0<r<\rho<R;\\ A_2 I_{\nu,\alpha}(\lambda r)+B_2 K_{\nu,\alpha}(\lambda r),\ 0<\rho<r<R,\end{cases}$$

where $I_{\nu,\alpha}(\lambda r)$, $K_{\nu,\alpha}(\lambda r)$ are modified Bessel functions of the first and second kind $\nu=ia^{-1}\beta$, $\operatorname{Re}\nu\ge\alpha\ge-\frac{1}{2}$, write down in the form:

$$p=-\left(\beta^2+\gamma^2\right)=\left(\beta^2+\gamma^2\right)e^{\pi i},$$

$$dp=-2\beta d\beta,\ \ b(\beta)=a^{-1}\beta.$$

Returning to the original, it is possible to obtain:

$$T(\tau,r)=\frac{a^{-2}}{2\pi i}\int_0^R\Big(\int_{\sigma_0-i\infty}^{\sigma_0+i\infty}\varepsilon_\alpha^*(p,r,\rho)e^{p\tau}dp\Big)g(\rho)\rho^{2\alpha-1}d\rho,$$

where a^{-2} is a weight function [20]. The special points of the Cauchy function $\varepsilon^*(p,r,\rho)$ are the branching points $p=-\gamma^2\le 0$ and the point $p=\infty$.

Let's denote:

$$X_{\alpha;11}^{11}(\lambda R,b)=\alpha_{11}^1\frac{d}{dr}C_\alpha(\lambda r,b)+\beta_{11}^1C_\alpha(\lambda r,b)\Big|_{r=R}=\alpha_{11}^1\lambda\left[\frac{dI_{i\beta,\alpha}(\lambda R)}{dr}+\frac{i}{\pi}sh\pi b\frac{dK_{i\beta,\alpha}(\lambda R)}{dr}\right]+$$

$$+\beta_{11}^1\left[I_{i\beta,\alpha}(\lambda R)+i\pi^{-1}sh\pi b\,K_{i\beta,\alpha}(\lambda R)\right]=\tilde{X}_{\alpha;11}^{11}(\lambda R)+i\frac{sh\pi b}{\pi}\tilde{X}_{\alpha;11}^{12}(\lambda R);$$

$$X_{\alpha;11}^{12}(\lambda R,b)=\left(\alpha_{11}^1\frac{d}{dr}+\beta_{11}^1\right)D_\alpha(\lambda r,b)\Big|_{r=R}=$$

$$=\alpha_{11}^1\lambda\left[\frac{1}{\pi}sh\pi b\frac{dK_{i\beta,\alpha}(\lambda R)}{dr}\right]+\beta_{11}^1\pi^{-1}sh\pi b\,K_{i\beta,\alpha}(\lambda R)=$$

$$=\pi^{-1}sh\pi b\left[\alpha_{11}^1\lambda\frac{d}{dr}K_{i\beta,\alpha}(\lambda R)+\beta_{11}^1K_{i\beta,\alpha}(\lambda R)\right]=\tilde{X}_{\alpha;11}^{12}(\lambda R)\frac{sh\pi b}{\pi};\qquad(1.8)$$

$$\tilde{X}^{11}_{\alpha;11}(\lambda R)=\alpha^1_{11}\lambda\frac{dI_{i\beta,\alpha}(\lambda R)}{dr}+\beta^1_{11}I_{i\beta,\alpha}(\lambda R);$$

$$\tilde{X}^{12}_{\alpha;11}(\lambda R)=\alpha^1_{11}\lambda\frac{dK_{i\beta,\alpha}(\lambda R)}{dr}+\beta^1_{11}K_{i\beta,\alpha}(\lambda R).$$

If to pass to the Bessel functions of a real argument $J_{\nu,\alpha}(\lambda R,b)$, $N_{\nu,\alpha}(\lambda R,b)$, then:

$$X^{11}_{\alpha;11}(\lambda R,b)=\left(\alpha^1_{11}\frac{\nu-\alpha}{R}+\beta^1_{11}\right)J_{\nu,\alpha}(\lambda R,b)-\alpha^1_{11}R\lambda^2J_{\nu+1,\alpha+1}(\lambda R,b),\ b=a^{-1}\beta;$$

$$X^{12}_{\alpha;11}(\lambda R,b)=\left(\alpha^1_{11}\frac{\nu-\alpha}{R}+\beta^1_{11}\right)N_{\nu,\alpha}(\lambda R,b)-\alpha^1_{11}R\lambda^2N_{\nu+1,\alpha+1}(\lambda R,b).$$

Let's determine functions:

$$U^{11}_{\nu,\alpha;11}(\lambda R,b)=X^{11}_{\alpha;11}(\lambda R,b)-i\,X^{12}_{\alpha;11}(\lambda R,b)=\tilde{X}^{11}_{\alpha,11}(\lambda R)=\alpha^1_{11}\lambda\frac{dI_{i\beta,\alpha}(\lambda R)}{dr}+\beta^1_{11}I_{i\beta,\alpha}(\lambda R)=$$

$$=\left(\alpha^1_{11}\frac{\nu-\alpha}{R}+\beta^1_{11}\right)I_{\nu,\alpha}(\lambda R,b)+\alpha^1_{11}R\lambda^2I_{\nu+1,\alpha+1}(\lambda R,b),\ \ \nu=a^{-1}\beta;$$

$$U^{12}_{\nu,\alpha;11}(\lambda R)=\pi(sh\,b\pi)^{-1}X^{12}_{\alpha,11}(\lambda R,b)=\left(\alpha^1_{11}\frac{d}{dr}+\beta^1_{11}\right)K_{\nu,\alpha}(\lambda r)\Big|_{r=R}=\tilde{X}^{12}_{\alpha,11}(\lambda R,b)=$$

$$=\left(\alpha^1_{11}\frac{\nu-\alpha}{R}+\beta^1_{11}\right)K_{\nu,\alpha}(\lambda R)+\alpha^1_{11}R\lambda^2K_{\nu+1,\alpha+1}(\lambda R). \qquad (1.9)$$

Satisfying the condition (1.7), it is possible to obtain the algebraic system of equations for determining the coefficients A_1, A_2, B_2:

$$(A_2-A_1)I_{\nu,\alpha}(\lambda\rho)+B_2K_{\nu,\alpha}(\lambda\rho)=0,$$

$$(A_2-A_1)I'_{\nu,\alpha}(\lambda\rho)+B_2K'_{\nu,\alpha}(\lambda\rho)=-\frac{1}{\lambda\rho^{2\alpha+1}}.$$

Given the relation:

$$I_{\nu,\alpha}(\lambda\rho)K'_{\nu,\alpha}(\lambda\rho)-I'_{\nu,\alpha}(\lambda\rho)K_{\nu,\alpha}(\lambda\rho)=-(\lambda\rho)^{-(2\alpha+1)},$$

let's obtain:

$$(A_2-A_1)=-\lambda^{2\alpha}K_{\nu,\alpha}(\lambda\rho),\ B_2=\lambda^{2\alpha}I_{\nu,\alpha}(\lambda\rho). \qquad (1.10)$$

CHAPTER 1

Satisfying the boundary condition for $r = R$, it is possible to obtain:

$$A_2 U^{11}_{\nu,\alpha;11}(\lambda R) + B_2 U^{12}_{\nu,\alpha;11}(\lambda R) = 0, \tag{1.11}$$

$$A_2 = \lambda^{2\alpha} \frac{\Psi^{1*}_{\nu,\alpha,11}(\lambda R, \lambda\rho)}{U^{11}_{\nu,\alpha,11}(\lambda R)} - \lambda^{2\alpha} K_{\nu,\alpha}(\lambda\rho) = \lambda^{2\alpha} \left\{ \frac{\Psi^{1*}_{\nu,\alpha,11}(\lambda R,\lambda\rho) - U^{11}_{\nu,\alpha,11}(\lambda R) K_{\nu,\alpha}(\lambda\rho)}{U^{11}_{\nu,\alpha,11}(\lambda R)} \right\} =$$

$$= -\lambda^{2\alpha} \frac{U^{12}_{\nu,\alpha,11}(\lambda R)}{U^{11}_{\nu,\alpha,11}(\lambda R)} I_{\nu,\alpha}(\lambda\rho) = -B_2 \frac{U^{12}_{\nu,\alpha,11}(\lambda R)}{U^{11}_{\nu,\alpha,11}(\lambda R)},$$

$$A_1 = \frac{B_2 K_{\nu,\alpha}(\lambda\rho)}{I_{\nu,\alpha}(\lambda\rho)} + A_2,$$

where

$$A_1 = \lambda^{2\alpha} \left(U^{11}_{\nu,\alpha;11}(\lambda R) \right)^{-1} \Psi^{1*}_{\nu,\alpha;11}(\lambda R, \lambda\rho);$$

$$U^{12}_{\nu,\alpha;11}(\lambda R) = \frac{A_2 \left(U^{11}_{\nu,\alpha;11}(\lambda R) \right)}{\lambda^{2\alpha} I_{\nu,\alpha}(\lambda r)};$$

$$\Psi^{1*}_{\nu,\alpha;11}(\lambda R, \lambda r) = U^{11}_{\nu,\alpha;11}(\lambda R) K_{\nu,\alpha}(\lambda r) - U^{12}_{\nu,\alpha;11}(\lambda R) I_{\nu,\alpha}(\lambda r).$$

Then the function $\varepsilon_\alpha^*(p,r,\rho)$ due to the symmetry relative to the diagonal $r = \rho$ has the form:

$$\varepsilon^*_\alpha(p,r,\rho) = \frac{\lambda^{2\alpha}}{U^{11}_{\nu,\alpha;11}(\lambda R, b)} \begin{cases} I_{\nu,\alpha}(\lambda r) \Psi^{1*}_{\nu,\alpha;11}(\lambda R, \lambda\rho), & 0 < r < \rho < R; \\ I_{\nu,\alpha}(\lambda\rho) \Psi^{1*}_{\nu,\alpha;11}(\lambda R, \lambda r), & 0 < \rho < r < R. \end{cases} \tag{1.12}$$

The roots $p_n = -\left(\beta_n^{\ 2} + \gamma^2\right)$ of the transcendental equation $U^{11}_{\nu,\alpha;11}(\lambda R, b) = 0$ are simple poles of $\varepsilon_\alpha^*(p,r,\rho)$.

Let' consider the transcendental equation:

$$\left(\alpha^1_{11} \frac{\nu - \alpha}{R} + \beta^1_{11} \right) I_{\nu,\alpha}(\lambda R, b) - \alpha^1_{11} \lambda^2 R I_{\nu+1,\alpha+1}(\lambda R, b) = 0,$$

where $p = -\left(\beta^2 + \gamma^2\right) = \left(\beta^2 + \gamma^2\right) e^{\pi i}$, $b(\beta) = a^{-1}\beta$ form a discrete spectrum $\{b_n\}_{n=1}^{\infty}$.

Let's denote $\Psi^1_{\nu,\alpha;11}(\lambda R, \lambda r, b) = \pi^{-1}(sh\,\pi b) \times \Psi^{1*}_{\nu,\alpha;11}(\lambda R, \lambda r, b)$.

Here $\Psi^{1}_{\nu,\alpha;11}(\lambda R,\lambda r,b)$ is the eigenfunction of the problem that satisfies equation (1.2) and homogeneous boundary conditions. It is possible to use it to construct a solution of the problem that satisfies the inhomogeneous condition at the outer surface of the cylinder, i.e., reflects the effect of the drying agent.

The original of the fundamental function:

$$\varepsilon_{\alpha}(t,r,\rho)=\int_{0}^{\infty} e^{-(\beta^{2}+\gamma^{2})t}\Psi^{1}_{\nu,\alpha;11}(\lambda R,\lambda r,b)\Psi^{1}_{\nu,\alpha;11}(\lambda R,\lambda\rho,b)\frac{2\beta\lambda^{2\alpha}d\beta}{\left(X^{11}_{\alpha;11}\right)^{2}+\left(X^{12}_{\alpha;11}\right)^{2}}=$$

$$=\int_{0}^{\infty} e^{-(\beta^{2}+\gamma^{2})t}V_{\alpha}(r,\beta)V_{\alpha}(\rho,\beta)\Omega_{\alpha}(\beta)d\beta; \qquad (1.13)$$

$$\Omega_{\alpha}(\beta)=\frac{2\beta\lambda^{2\alpha}}{\left(X^{11}_{\alpha;11}(\lambda R,\beta)\right)^{2}+\left(X^{12}_{\alpha;11}(\lambda R,\beta)\right)^{2}}.$$

By the generalized development theorem:

$$\varepsilon_{\alpha}(t,r,\rho)=\sum_{n=1}^{\infty} e^{-(\beta_{n}^{2}+\gamma^{2})t}\frac{V_{\alpha}(b_{n}r)V_{\alpha}(b_{n}\rho)}{\left\|V_{\alpha}(b_{n}r)\right\|_{1}^{2}},$$

where $\left\|V_{\alpha}(b_{n}r)\right\|_{1}^{2}$ is the square of the norm of its own function; b_n are roots of the function $U^{11}_{\nu,\alpha;11}(\lambda R,b)$.

$$\Psi^{1*}_{\nu,\alpha;11}(i\lambda R,i\lambda\rho)=-\frac{\pi}{2}e^{-\pi i\alpha}\Psi^{1}_{\nu,\alpha;11}(\lambda R,\lambda\rho),$$

$$V_{\alpha}(r,\beta)=\Psi^{1}_{\alpha;11}(\lambda R,\lambda r,\beta)=X^{11}_{\alpha;11}(\lambda R,\beta)D_{\alpha}(\lambda r,\beta)-X^{12}_{\alpha;11}(\lambda R,\beta)C_{\alpha}(\lambda r,\beta), \qquad (1.14)$$

$$\Psi^{*1}_{\nu,\alpha;11}(i\lambda R,i\lambda r)=-\frac{\pi}{2}e^{-\pi i\alpha}\Psi^{1}_{\nu,\alpha;11}(\lambda R,\lambda r).$$

Here $V_{\alpha}(r,\beta)=\Psi^{1}_{\alpha;11}(\lambda R,\lambda r,\beta)$ is eigenfunction (spectral function) of the problem (1.6); $\Omega_{\alpha}(\beta)$ is a spectral density.

Returning in equation (1.13) to the original, it is possible to obtain a solution $T_{odn}(t,r)$ of the homogeneous parabolic Cauchy problem (1.2), (1.3):

$$T_{odn}(t,r)=\int_{0}^{R}\varepsilon_{\alpha}(t,r,\rho)g(\rho)\rho^{2\alpha-1}a^{-2}d\rho=$$

$$=\int_0^\infty e^{-\left(\beta^2+\gamma^2\right)t}V_\alpha\left(r,\beta\right)\int_0^R g\left(\rho\right)V_\alpha\left(\rho,\beta\right)\sigma\rho^{2\alpha-1}d\rho\Omega_\alpha\left(\beta\right)d\beta,\ \sigma=a^{-2}. \tag{1.15}$$

From equation (1.15) for $t = 0$, it is possible to obtain the integral image:

$$g\left(r\right)=\int_0^\infty V_\alpha\left(r,\beta\right)\int_0^R g\left(\rho\right)V_\alpha\left(\rho,\beta\right)\sigma\rho^{2\alpha-1}d\rho\Omega_\alpha\left(\beta\right)d\beta. \tag{1.16}$$

From equation (1.16), it follows that the function $\varepsilon_\alpha(t,r,\rho)$ defined by equation (1.13) is a delta-shaped sequence with respect to t for $t\to 0+$.

The integral image (1.16) defines a direct:

$$H_\alpha\left[g\left(r\right)\right]=\int_0^R g\left(r\right)V_\alpha\left(r,\beta\right)\sigma r^{2\alpha-1}dr\equiv\tilde{g}\left(\beta\right); \tag{1.17}$$

and inverse:

$$H^{-1}{}_\alpha\left[\tilde{g}\left(r\right)\right]=\int_0^\infty\tilde{g}\left(\beta\right)V_\alpha\left(r,\beta\right)\Omega_\alpha\left(\beta\right)d\beta\equiv g\left(r\right). \tag{1.18}$$

Kontorovich-Lebedev transform over the interval [0, R].

Given the theorem on the basic identity of the integral transform [20] of a differential operator B_α, i.e., if the function $g(r)$ is such that the function $f(r) = B_\alpha[g(R)]$ is continuous on the set (0, R) and the boundary conditions hold:

$$\lim_{r\to 0} r^{2\alpha+1}\left(\frac{dg}{dr}V_\alpha\left(r,\beta\right)-g\left(r\right)\frac{dV_\alpha}{dr}\right)=0,\ \left(\alpha_{11}^1\frac{d}{dr}+\beta_{11}^1\right)g\left(r\right)\Big|_{r=R}=g_R\left(\tau\right), \tag{1.19}$$

then for any $\lambda\in\left(0,\infty\right)$, the following equality holds:

$$H_\alpha\left[a^2B_\alpha\left[g\left(r\right)\right]\right]=-\beta^2\tilde{g}\left(\beta\right)+\frac{sh\,\pi\beta}{\pi\lambda^{2\alpha}}g_R\left(\tau\right). \tag{1.20}$$

Therefore, based on relation (1.17), it follows:

$$H_\alpha\left[a^2B_\alpha\left[g\left(r\right)\right]\right]=-\beta^2\int_0^R g\left(r\right)V_\alpha\left(r,\beta\right)\sigma r^{2\alpha-1}dr+\frac{sh\pi\beta}{\pi\lambda^{2\alpha}}T_a\left(R,\tau\right). \tag{1.21}$$

From the properties of the eigenfunction $V_\alpha(r,\beta)$, it follows that:

$$\left.\left(\alpha_{11}^{1}\frac{dV_\alpha(r,\beta)}{dr}+\beta_{11}^{1}V_\alpha(r,\beta)\right)\right|_{r=R}=0,\ \left(a^2B_\alpha+\beta^2\right)V_\alpha(r,\beta)=0.$$

From equation (1.21), taking into account equation (1.19), it is possible to obtain:

$$H_\alpha\left[a^2B_\alpha\left[g(r)\right]\right]=a^2\int_0^R B_\alpha\left[g(r)\right]V_\alpha(r,\beta)\sigma r^{2\alpha-1}dr=$$

$$=\int_0^R\left[r^2\frac{d^2g}{dr^2}+(2\alpha+1)r\frac{dg}{dr}-\lambda^2r^2g(r)+\alpha^2g(r)\right]V_\alpha(r,\beta)r^{2\alpha-1}dr=$$

$$=a^2\sigma r^{2\alpha+1}\left[g'(r)V_\alpha(r,\beta)-g(r)V_\alpha'(r,\beta)\right]\Big|_0^R+\int_0^R g(r)a^2\sigma B_\alpha\left[V_\alpha(r,\beta)\right]r^{2\alpha-1}dr=$$

$$=R^{2\alpha+1}\left[g'(r)V_\alpha(r,\beta)-g(r)V_\alpha'(r,\beta)\right]\Big|_{r=R}-\beta^2H_\alpha\left[g(r)\right].$$

where $H_\alpha[g(r)]$ is defined by the expression (1.17); $g_R=T_{aR}(R,t)$ is the temperature of the drying agent.

Then from equation (1.21), it is possible to obtain:

$$\frac{g_R}{\alpha_{11}^{1}}V_\alpha(R,\beta)=\frac{g_R}{\alpha_{11}^{1}}\left[X_{\alpha;11}^{11}(\lambda R,b)D_\alpha(\lambda R,b)-X_{\alpha;11}^{12}(\lambda R,b)C_\alpha(\lambda R,b)\right]=$$

$$=g_R\left[C_{r\alpha}'(\lambda R,b)D_\alpha(\lambda R,b)-D_{r\alpha}'(\lambda R,b)C_\alpha(\lambda R,b)\right]=\frac{sh\pi b}{\pi\lambda^{2\alpha}R^{2\alpha+1}}T_{aR}. \tag{1.22}$$

The equations of thermal conductivity and boundary conditions have the following form:

$$\frac{\partial T}{\partial\tau}+\left(\beta^2+\gamma^2\right)T=0;\ T(\tau,\beta)\big|_{\tau=0}=g(\beta),\ \left(\alpha_{11}^{1}\frac{d}{dr}+\beta_{11}^{1}\right)T(r)\big|_{r=R}=T_{aR}(\tau).$$

As a result of identity (1.21):

$$\frac{\partial\tilde{T}}{\partial\tau}+\left(\beta^2+\gamma^2\right)\tilde{T}=\frac{sh\pi b}{\pi\lambda^{2\alpha}}T_{aR}(\tau);\ \ \tilde{T}(\tau,\beta)\big|_{\tau=0}=\tilde{g}(\beta). \tag{1.23}$$

The solution of the Cauchy problem (1.23) is the function:

$$\tilde{T}(\tau,\beta)=e^{-\left(\beta^2+\gamma^2\right)\tau}\tilde{g}(\beta)+\int_0^\tau e^{-\left(\beta^2+\gamma^2\right)(\tau-t)}\left[\frac{sh\pi b}{\pi\lambda^{2\alpha}}\left(\alpha_0+\sum_{n=1}^{\infty}\alpha_n\cos\nu_n^2t\right)\right]dt. \tag{1.24}$$

Let's apply the integral operator H_α^{-1} (1.18) to $\tilde{T}(\tau,\beta)$, and obtain the solution of the problem (1.24):

$$T(t,r)=\int_0^t\int_0^R\int_0^\infty e^{-(\beta^2+\gamma^2)(t-\tau)}V_\alpha(r,\beta)V_\alpha(\rho,\beta)\Omega_\alpha(\beta)d\beta\left[\delta_+(\tau)g(\rho)\right]\sigma\rho^{2\alpha-1}d\rho d\tau+$$

$$+\int_0^\infty\int_0^t e^{-(\beta^2+\gamma^2)(t-\tau)}\frac{sh\pi b}{\pi\lambda^{2\alpha}}T_a(\tau)V_\alpha(r,\beta)\Omega_\alpha(\beta)d\beta d\tau. \tag{1.25}$$

From equations (1.17), (1.18) and Steklov's theorem, any vector-function $f(r) = B_\alpha[g(r)]$ continuous on $(0,R)$ satisfying zero boundary conditions can be decomposed in terms of a system of eigenfunctions $V_\alpha(r,\beta_j)_{j=1}^{\infty}$ into an absolutely and uniformly convergent Fourier series.

It is known that one eigenvector-function $V_\alpha(r,\beta_j)$ corresponds to each eigenvalue β_j and the system of spectral functions $V_\alpha(r,\beta_j)_{j=1}^{\infty}$ is complete and closed. The square of the norm of eigenfunction $\left\|V_\alpha(r,\beta_j)\right\|^2=\int_0^R\left[V_\alpha(r,\beta_j)\right]^2\sigma r^{2\alpha-1}dr.$

Thus, given equation (1.17), the inverse integral operator (1.18) can be written down as follows:

$$H_\alpha^{-1}\left[\tilde{g}(r)\right]=\sum_{j=0}^{\infty}\tilde{g}(\beta_j)V_\alpha(r,\beta_j)\left(\left\|V_\alpha(r,\beta_j)\right\|^2\right)^{-1}\equiv g(r),$$

and the function:

$$G_\alpha(t,r,\rho)=\int_0^\infty e^{-(\beta^2+\gamma^2)t}V_\alpha(r,\beta)V_\alpha(\rho,\beta)\Omega_\alpha(\beta)d\beta, \tag{1.26}$$

by taking into account the initial temperature state of the body, according to the theory of surpluses can be represented as calculated integral in the form:

$$G_\alpha(t,r,\rho)=\sum_{j=1}^{\infty} e^{-(\beta_j^2+\gamma^2)t}\frac{V_\alpha(r,\beta_j)V_\alpha(\rho,\beta_j)}{\left\|V_\alpha(r,\beta_j)\right\|^2}\sigma a^2,$$

where

$$V_\alpha(r,\beta_j)=\Psi^1{}_{\alpha;11}(\lambda R,\lambda r,\beta_j)=\frac{sh\pi\beta_j}{\pi}\left[X_{\alpha;11}^{11}(\lambda R,\beta_j)D_\alpha(\lambda r,\beta_j)-X_{\alpha;11}^{12}(\lambda R,\beta_j)C_\alpha(\lambda r,\beta_j)\right];$$

as well as the Green's function generated by the thermal regime at the boundary:

$r = R$;

$$W_\alpha(t,r) = \int_0^\infty e^{-(\beta^2+\gamma^2)t} V_\alpha(r,\beta) \frac{sh\pi\beta}{\pi\lambda^{2\alpha}} \Omega_\alpha(\beta) d\beta, \; b = a^{-1}\beta;$$

$$W_\alpha(t,r) = \sum_{j=1}^\infty e^{-(\beta_j^2+\gamma^2)t} \frac{sh\pi\beta_j}{\pi\lambda^{2\alpha}} \frac{V_\alpha(r,\beta_j)}{\left\| V_\alpha(r,\beta_j) \right\|^2} \sigma a^2. \qquad (1.27)$$

Then the solution will take the form:

$$T(t,r) = \int_0^t \int_0^R G_\alpha(t-\tau,r,\rho)\left[\delta_+(\tau) g(\rho)\right] \sigma\rho^{2\alpha-1} d\rho d\tau + \int_0^t W_\alpha(t-\tau,r) T_a(\tau) d\tau. \qquad (1.28)$$

Here $\delta_+(t)$ is a delta-function concentrated at the point $0+$.

According to equation (1.28), taking into account the properties of delta-function and equation (1.17), it is possible to obtain:

$$T(t,r) = \int_0^\infty e^{-(\beta^2+\gamma^2)t} \tilde{g}(\beta) V_\alpha(r,\beta) \Omega_\alpha(\beta) d\beta + \int_0^\infty \int_0^t e^{-(\beta^2+\gamma^2)(t-\tau)} \frac{sh\pi\beta}{\pi\lambda^{2\alpha}} T_{aR}(\tau) V_\alpha(r,\beta) \Omega_\alpha(\beta) d\beta.$$

Let's denote $\int_0^t e^{-(\beta^2+\gamma^2)(t-\tau)} \frac{sh\pi b}{\pi\lambda^{2\alpha}} T_{aR}(\tau) d\tau = T_{wa}(t,\beta)$. It is possible to transit to improper integrals:

$$T(t,r) = \int_0^\infty e^{-(\beta^2+\gamma^2)t} \tilde{g}(\beta) V_\alpha(r,\beta) \Omega_\alpha(\beta) d\beta + \int_0^\infty T_{wa}(\tau,\beta) V_\alpha(r,\beta) \Omega_\alpha(\beta) d\beta.$$

Taking into account equation (1.26), (1.27), let's obtain:

$$T(t,r) = \sum_{j=1}^\infty e^{-(\beta_j^2+\gamma^2)t} \tilde{g}(\beta_j) \frac{V_\alpha(r,\beta_j)}{\left\| V_\alpha(r,\beta_j) \right\|^2} \sigma a^2 + \sum_{j=1}^\infty T_{wa}(\tau,\beta_j) \frac{V_\alpha(r,\beta_j)}{\left\| V_\alpha(r,\beta_j) \right\|^2} \sigma a^2.$$

Let's determine the effect of initial conditions and temperature of the drying agent on the drying process. Given equation (1.16), the initial condition $\left(g(r) = \sum_{j=0}^{2} g_{j0} r^j \right)$ is chosen. Then:

$$\tilde{g}(\beta)=\frac{1}{a^2}\int_0^R\sum_{j=0}^{2}\left(g_{j0}r^{j+2\alpha-1}\right)\times\left[X_{\alpha 11;}^{11}(\lambda R,\beta)\left(\pi^{-1}sh\pi\beta K_{i\beta,\alpha}(\lambda r)\right)-\right.$$

$$\left.-X_{\alpha 11;}^{12}(\lambda R,\beta)\left(I_{i\beta,\alpha}(\lambda r)+i\left(\pi^{-1}sh\pi\beta K_{i\beta,\alpha}(\lambda r)\right)\right)\right]dr.$$

Given expressions for the Bessel functions:

$$I_{\nu,\alpha}(\lambda\rho)=(\lambda\rho)^{-\alpha}I_\nu(\lambda\rho),\ \ K_{\nu,\alpha}(\lambda\rho)=(\lambda\rho)^{-\alpha}K_\nu(\lambda\rho).$$

Let's determine:

$$\tilde{g}(\beta)=\frac{1}{a^2}\left\{\begin{array}{l}X_{\alpha 11;}^{11}(\lambda R,\beta)\pi^{-1}sh\pi\beta\int_0^R\sum_{j=0}^{2}\left(g_{j0}r^{j+\alpha-1}\right)K_{i\beta}(\lambda r)dr-\\ -X_{\alpha 11;}^{12}(\lambda R,\beta)\int_0^R\sum_{j=0}^{2}\left(g_{j0}r^{j+\alpha-1}\right)I_{i\beta}(\lambda r)dr-\\ -iX_{\alpha 11;}^{12}(\lambda R,\beta)\pi^{-1}sh\pi\beta\int_0^R\sum_{j=0}^{2}\left(g_{j0}r^{j+\alpha-1}\right)K_{i\beta}(\lambda r)dr\end{array}\right\}=$$

$$=\frac{1}{a^2}\left\{\begin{array}{l}\left[X_{\alpha 11;}^{11}(\lambda R,\beta)-iX_{\alpha 11;}^{12}(\lambda R,\beta)\right]\pi^{-1}sh\pi\beta\int_0^{\lambda R}\sum_{j=0}^{2}\lambda^{-(2\alpha+j)}\left(g_{j0}r^{j+\alpha-1}\right)K_{i\beta}(\lambda r)dr-\\ -X_{\alpha 11;}^{12}(\lambda R,\beta)\int_0^{\lambda R}\sum_{j=0}^{2}\lambda^{-(2\alpha+j)}\left(g_{j0}r^{j+\alpha-1}\right)I_{i\beta}(r)dr\end{array}\right\}.$$

$$\tilde{T}_{go}(\tau,\beta)=e^{-\left(\beta^2+\gamma^2\right)\tau}\left\langle\frac{1}{a^2}U_{\alpha,11}^{11}(\lambda R)\pi^{-1}sh\pi\beta\lambda^{-\alpha}\sum_{j=0}^{2}g_{j0}\frac{1}{\lambda^{j+\alpha}}\times\right.$$

$$\times\left\{\frac{2^{i\beta-1}\Gamma(i\beta)}{j+\alpha-i\beta}(\lambda R)^{j+\alpha-i\beta}{}_1F_2\left(\frac{j+\alpha-i\beta}{2};1-i\beta;\frac{j+\alpha-i\beta+2}{2},\frac{(\lambda R)^2}{4}\right)+\right.$$

$$\left.\left.\frac{2^{-i\beta-1}\Gamma(-i\beta)}{j+\alpha+i\beta}(\lambda R)^{j+\alpha+i\beta}{}_1F_2\left(\frac{j+\alpha+i\beta}{2};1+i\beta;\frac{j+\alpha+i\beta+2}{2},\frac{(\lambda R)^2}{4}\right)\right\}\right\}-X_{\alpha 11;}^{12}(\lambda R,\beta)\frac{\lambda^{-\alpha}}{a^2}\times$$

$$\times\sum_{j=0}^{2}g_{j0}\frac{1}{\lambda^{j+\alpha}}\left\{\frac{1}{2^{i\beta}(j+\alpha+i\beta)\Gamma(1+i\beta)}(\lambda R)^{j+\alpha+i\beta}{}_1;\right.$$

$$F_2\left(\frac{j+\alpha+i\beta}{2};\frac{j+\alpha+i\beta+2}{2},1+i\beta;\frac{(\lambda R)^2}{4}\right)\Bigg\}\Bigg\}\Bigg\rangle.$$

Here ${}_1F_2\left((a_1)_k;(b_1)_k,(b_2)_k;z\right)=\sum_{k=0}^{\infty}\frac{(a_1)_k}{(b_1)_k(b_2)_k}\frac{z^k}{k!}$ are generalized hypergeometric function, where $(a_1)_k=\frac{j+\alpha\pm i\beta}{2}$; $(b_1)_k=\frac{j+\alpha\pm i\beta+2}{2}$; $(b_2)_k=1\pm i\beta$; $z=\frac{(\lambda R)^2}{4}$ are Pochhammer's polynomials [21]. Let's write these functions.

Let's write the first of these functions:

$$(a_1)_k=\frac{j+\alpha-i\beta}{2};\ (b_1)_k=1-i\beta;\ (b_2)_k=\frac{j+\alpha-i\beta+2}{2};\ z=\frac{(\lambda R)^2}{4};$$

$$\Phi_1={}_1F_2\left(\frac{j+\alpha-i\beta}{2};1-i\beta;\frac{j+\alpha-i\beta+2}{2},\frac{(\lambda R)^2}{4}\right)=1+\frac{\left(\frac{j+\alpha-i\beta}{2}\right)\frac{(\lambda R)^2}{4}}{(1-i\beta)\left(\frac{j+\alpha-i\beta+2}{2}\right)1!}+$$

$$+\frac{\left(\frac{j+\alpha-i\beta}{2}\right)\left(\frac{j+\alpha-i\beta}{2}+1\right)\left(\frac{(\lambda R)^2}{4}\right)^2}{(1-i\beta)(1-i\beta+1)\left(\frac{j+\alpha-i\beta+2}{2}\right)\left(\frac{j+\alpha-i\beta+2}{2}+1\right)2!}+$$

$$+\frac{\left(\frac{j+\alpha-i\beta}{2}\right)\left(\frac{j+\alpha-i\beta}{2}+1\right)\left(\frac{j+\alpha-i\beta}{2}+2\right)\left(\frac{(\lambda R)^2}{4}\right)^3}{(1-i\beta)(1-i\beta+1)(1-i\beta+2)\left(\frac{j+\alpha-i\beta+2}{2}\right)\left(\frac{j+\alpha-i\beta+2}{2}+1\right)\left(\frac{j+\alpha-i\beta+2}{2}+2\right)3!}+\dots.$$

The second function:

$$(a_1)_k=\frac{j+\alpha+i\beta}{2};\ (b_1)_k=1+i\beta;\ (b_2)_k=\frac{j+\alpha+i\beta+2}{2};\ z=\frac{(\lambda R)^2}{4};$$

$$\Phi_2={}_1F_2\left(\frac{j+\alpha+i\beta}{2};1+i\beta,\frac{j+\alpha+i\beta+2}{2};\frac{(\lambda R)^2}{4}\right)=1+\frac{\left(\frac{j+\alpha+i\beta}{2}\right)\frac{(\lambda R)^2}{4}}{(1+i\beta)\left(\frac{j+\alpha+i\beta+2}{2}\right)1!}+$$

$$+\frac{\left(\frac{j+\alpha+i\beta}{2}\right)\left(\frac{j+\alpha+i\beta}{2}+1\right)\left(\frac{(\lambda R)^2}{4}\right)^2}{(1+i\beta)(1+i\beta+1)\left(\frac{j+\alpha+i\beta+2}{2}\right)\left(\frac{j+\alpha+i\beta+2}{2}+1\right)2!}+$$

$$+\frac{\left(\frac{j+\alpha+i\beta}{2}\right)\left(\frac{j+\alpha+i\beta}{2}+1\right)\left(\frac{j+\alpha+i\beta}{2}+2\right)\left(\frac{(\lambda R)^2}{4}\right)^3}{(1+i\beta)(1+i\beta+1)(1+i\beta+2)\left(\frac{j+\alpha+i\beta+2}{2}\right)\left(\frac{j+\alpha+i\beta+2}{2}+1\right)\left(\frac{j+\alpha+i\beta+2}{2}+2\right)3!}+\dots.$$

The third function [21]:

$$(a_1)_k=\frac{j+\alpha+i\beta}{2};\ (b_1)_k=\frac{j+\alpha+i\beta+2}{2};\ (b_2)_k=1+i\beta;\ \ z=\frac{(\lambda R)^2}{4};$$

$$\Phi_3={}_1F_2\left(\frac{j+\alpha+i\beta}{2};\frac{j+\alpha+i\beta+2}{2},1+i\beta;\frac{(\lambda R)^2}{4}\right)=1+\frac{\left(\frac{j+\alpha+i\beta}{2}\right)\frac{(\lambda R)^2}{4}}{\left(\frac{j+\alpha+i\beta+2}{2}\right)(1+i\beta)1!}+$$

$$+\frac{\left(\frac{j+\alpha+i\beta}{2}\right)\left(\frac{j+\alpha+i\beta}{2}+1\right)\left(\frac{(\lambda R)^2}{4}\right)^2}{\left(\frac{j+\alpha+i\beta+2}{2}\right)\left(\frac{j+\alpha+i\beta+2}{2}+1\right)(1+i\beta)(1+i\beta+1)\cdot 2!}+$$

$$+\frac{\left(\frac{j+\alpha+i\beta}{2}\right)\left(\frac{j+\alpha+i\beta}{2}+1\right)\left(\frac{j+\alpha+i\beta}{2}+2\right)\left(\frac{(\lambda R)^2}{4}\right)^3}{\left(\frac{j+\alpha+i\beta+2}{2}\right)\left(\frac{j+\alpha+i\beta+2}{2}+1\right)\left(\frac{j+\alpha+i\beta+2}{2}+2\right)(1+i\beta)(1+i\beta+1)(1+i\beta+2)\cdot 3!}+\dots.$$

Comparing the expressions for Φ_2 and Φ_3, it is possible to see that $\Phi_2=\Phi_3$. Let's consider the expressions of the first three coefficients of each of these generalized hypergeometric functions. Let's determine the real and imaginary parts in them. Let's consider the function:

$$\Phi_1={}_1F_2\left(\frac{j+\alpha-i\beta}{2};1-i\beta;\frac{j+\alpha-i\beta+2}{2},\frac{(\lambda R)^2}{4}\right)={}_1F_2\left(a_1+a_1^i i;b_1+b_1^i i;b_2+b_2^i i\right)=$$

$$=1+A_1+A_2+A_3\dots.$$

Let's introduce the denotations:

$$(a_1)_k = \frac{j+\alpha-i\beta}{2};\ (b_1)_k = 1-i\beta;\ (b_2)_k = \frac{j+\alpha-i\beta+2}{2};\ z = \frac{(\lambda R)^2}{4};$$

$$a_1 = \frac{j+\alpha}{2};\ a_1^i = -\frac{\beta}{2};\ b_1 = 1;\ b_1^i = -\beta;\ b_2 = \frac{j+\alpha+2}{2};\ b_2^i = -\frac{\beta}{2}.$$

Here

$$A_1 = \frac{\frac{j+\alpha-i\beta}{2}\frac{(\lambda R)^2}{4}}{(1-i\beta)\frac{j+\alpha-i\beta+2}{2}} = A_{11} + A_{11}^i i,$$

where

$$A_{11} = \frac{\left\{a_1\left(b_1b_2 - b_1^ib_2^i\right) + a_1^i\left(b_1b_2^i + b_1^ib_2\right)\right\}}{\left[\left(b_1^2 + b_1^{i2}\right)\left(b_2^2 + b_2^{i2}\right)\right]}\frac{(\lambda R)^2}{4},$$

$$A_{11}^i = \frac{\left\{a_1^i\left(b_1b_2 - b_1^ib_2^i\right) - a_1\left(b_1b_2^i + b_1^ib_2\right)\right\}}{\left[\left(b_1^2 + b_1^{i2}\right)\left(b_2^2 + b_2^{i2}\right)\right]}\frac{(\lambda R)^2}{4};$$

$$A_2 = \frac{\left(\frac{j+\alpha-i\beta}{2}\right)\left(\frac{j+\alpha-i\beta}{2}+1\right)\left(\frac{(\lambda R)^2}{4}\right)^2}{(1-i\beta)(1-i\beta+1)\left(\frac{j+\alpha-i\beta+2}{2}\right)\left(\frac{j+\alpha-i\beta+2}{2}+1\right)2!} = A_{12} + A_{12}^i i =$$

$$= \left(A_{11} + A_{11}^i i\right)\left\langle\left\{\left[(b_1+1)(b_2+1) - b_1^ib_2^i\right]a_1 + a_1^i\left[(b_1+1)b_2^i + b_1^i(b_2+1)\right]\right\} + \right.$$

$$\left. + \left\{\left[(b_1+1)(b_2+1) - b_1^ib_2^i\right]a_1^i - \left[(b_1+1)b_2^i + b_1^i(b_2+1)\right]a_1\right\}i\right\rangle \times$$

$$\times \frac{\frac{(\lambda R)^2}{4}}{\left[\left((b_1+1)^2 + b_1^{i2}\right)\left((b_2+1)^2 + b_2^{i2}\right)\right]2};$$

$$A_{12} = \frac{\left\{\left[\left(b_1+1\right)\left(b_2+1\right)-b_1^i b_2^i\right]a_1 + a_1^i\left[\left(b_1+1\right)b_2^i + b_1^i\left(b_2+1\right)\right]\right\}}{\left[\left(\left(b_1+1\right)^2 + b_1^{i2}\right)\left(\left(b_2+1\right)^2 + b_2^{i2}\right)\right]2}\frac{\left(\lambda R\right)^2}{4},$$

$$A_{12}^i = \frac{\left\{\left[\left(b_1+1\right)\left(b_2+1\right)-b_1^i b_2^i\right]a_1^i - \left[\left(b_1+1\right)b_2^i + b_1^i\left(b_2+1\right)\right]a_1\right\}}{\left[\left(\left(b_1+1\right)^2 + b_1^{i2}\right)\left(\left(b_2+1\right)^2 + b_2^{i2}\right)\right]2}\frac{\left(\lambda R\right)^2}{4};$$

$$\left(A_2 + A_2^i i\right) = \left(A_{11} + A_{11}^i i\right)\left(A_{12} + A_{12}^i i\right) = \left(A_{11}A_{12} - A_{11}^i A_{12}^i\right) + \left(A_{11}A_{12}^i + A_{12}A_{11}^i\right)i;$$

$$A_3 = \frac{\left(\frac{j+\alpha-i\beta}{2}\right)\left(\frac{j+\alpha-i\beta}{2}+1\right)\left(\frac{j+\alpha-i\beta}{2}+2\right)\left(\frac{\left(\lambda R\right)^2}{4}\right)^3}{\left(1-i\beta\right)\left(1-i\beta+1\right)\left(1-i\beta+2\right)\left(\frac{j+\alpha-i\beta+2}{2}\right)\left(\frac{j+\alpha-i\beta+2}{2}+1\right)\left(\frac{j+\alpha-i\beta+2}{2}+2\right)3!} + \ldots =$$

$$= A_1A_2\left(A_{13} + A_{13}^i i\right) = A_1A_2\left\langle\left\{\left[\left(b_1+2\right)\left(b_2+2\right)-b_1^i b_2^i\right]a_1 + a_1^i\left[\left(b_1+2\right)b_2^i + b_1^i\left(b_2+2\right)\right]\right\} + \right.$$

$$\left. + \left\{\left[\left(b_1+2\right)\left(b_2+2\right)-b_1^i b_2^i\right]a_1^i - \left[\left(b_1+2\right)b_2^i + b_1^i\left(b_2+2\right)\right]a_1\right\} i\right\rangle \frac{\frac{\left(\lambda R\right)^2}{4}}{\left[\left(\left(b_1+2\right)^2 + b_2^{i2}\right)\left(\left(b_2+2\right)^2 + b_2^{i2}\right)\right]3!}.$$

$$\left(A_3 + A_3^i i\right) = \left(A_{11} + A_{11}^i i\right)\left(A_{12} + A_{12}^i i\right).\left(A_{13} + A_{13}^i i\right) =$$
$$= \left[\left(A_{11}A_{12} - A_{11}^i A_{12}^i\right)A_{13} - \left(A_{11}A_{12}^i + A_{12}A_{11}^i\right)A_{13}^i\right] + \left[\left(A_{11}A_{12} - A_{11}^i A_{12}^i\right)A_{13}^i - \left(A_{11}A_{12}^i + A_{12}A_{11}^i\right)A_{13}\right]i.$$

For the functions Φ_2, Φ_3, the representation of the coefficients A_1, A_2, $A_3 \ldots$ remain the same:

$$\Phi_2 = {}_1F_2\left(\frac{j+\alpha+i\beta}{2};1+i\beta;\frac{j+\alpha+i\beta+2}{2},\frac{\left(\lambda R\right)^2}{4}\right) = {}_1F_2\left(a_1 + a_1^i i; b_1 + b_1^i i; b_2 + b_2^i i; \frac{\left(\lambda R\right)^2}{4}\right) =$$

$$= 1 + \left(A_1 + A_1^i i\right) + \left(A_2 + A_2^i i\right) + \left(A_3 + A_3^i i\right) + \ldots,$$

$$a_1 = \frac{j+\alpha}{2};\ a_1^i = +\frac{\beta}{2};\ b_1 = 1;\ b_1^i = +\beta;\ b_2 = \frac{j+\alpha+2}{2};\ b_2^i = +\frac{\beta}{2};$$

$$\Phi_3 = {}_1F_2\left(\frac{j+\alpha+i\beta}{2};\frac{j+\alpha+i\beta+2}{2},1+i\beta;\frac{\left(\lambda R\right)^2}{4}\right) = {}_1F_2\left(a_1 + a_1^i i; b_1 + b_1^i i; b_2 + b_2^i i\right),$$

$$a_1 = \frac{j+\alpha}{2};\ a_1^i = \frac{\beta}{2};\ b_1 = \frac{j+\alpha+2}{2};\ b_1^i = \frac{\beta}{2};\ b_2 = 1;\ b_2^i = \beta.$$

Thus, recurrent relations are obtained for real and imaginary parts of generalized hypergeometric functions of complex arguments, which allows to determine the temperature distribution depending on the parameters of the structure of wood and other porous materials.

Let's determine the solution $\tilde{T}_{wa}(\beta)$ caused by the drying agent $\tilde{T}_{wa} = \frac{sh\pi b}{\pi\lambda^{2\alpha}} \int_0^\tau e^{-(\beta^2+\gamma^2)(\tau-t)} T_a(t)dt.$

$$\tilde{T}_{wa}(\tau) = \int_0^\tau e^{-(\beta^2+\gamma^2)(\tau-t)} \left[\frac{sh\pi b}{\pi\lambda^{2\alpha}} \left(\alpha_0 + \sum_{n=1}^{\infty} \alpha_n \cos\nu_n^2 t \right) \right] dt =$$

$$= e^{-(\beta^2+\gamma^2)\tau} \frac{sh\pi b}{\pi\lambda^{2\alpha}} \left[\frac{e^{(\beta^2+\gamma^2)t}}{(\beta^2+\gamma^2)} a_0 + \sum_{n=1}^{\infty} a_n \frac{e^{(\beta^2+\gamma^2)t}\left[(\beta^2+\gamma^2)\cos\nu_n^2 t + \nu_n^2 \sin\nu_n^2 t \right]}{(\beta^2+\gamma^2)^2 + (\nu_n^2)^2} \right] \Bigg|_0^\tau =$$

$$= e^{-(\beta^2+\gamma^2)\tau} \frac{sh\pi b}{\pi\lambda^{2\alpha}} \left[\frac{e^{(\beta^2+\gamma^2)\tau} - 1}{(\beta^2+\gamma^2)} a_0 + \right.$$

$$\left. + \sum_{n=1}^{\infty} a_n \frac{e^{(\beta^2+\gamma^2)\tau}\left[(\beta^2+\gamma^2)\cos\nu_n^2\tau + \nu_n^2 \sin\nu_n^2\tau \right] - (\beta^2+\gamma^2)}{(\beta^2+\gamma^2)^2 + (\nu_n^2)^2} \right] =$$

$$= \frac{sh\pi b}{\pi\lambda^{2\alpha}} \left[\frac{1 - e^{-(\beta^2+\gamma^2)\tau}}{(\beta^2+\gamma^2)} a_0 + \sum_{n=1}^{\infty} a_n \frac{\left[(\beta^2+\gamma^2)\cos\nu_n^2\tau + \nu_n^2 \sin\nu_n^2\tau \right] - e^{-(\beta^2+\gamma^2)\tau}(\beta^2+\gamma^2)}{(\beta^2+\gamma^2)^2 + (\nu_n^2)^2} \right]. \quad (1.31)$$

The solution of a Cauchy problem is the function:

$$\tilde{T}(\tau,\beta) = e^{-(\beta^2+\gamma^2)\tau} \tilde{g}(\beta) + \int_0^\tau e^{-(\beta^2+\gamma^2)(\tau-t)} \left[\frac{sh\pi b}{\pi\lambda^{2\alpha}} \left(\alpha_0 + \sum_{n=1}^{\infty} \alpha_n \cos\nu_n^2 t \right) \right] dt =$$

$$= e^{-(\beta^2+\gamma^2)\tau} \tilde{g}(\beta) + \tilde{T}_{wa}(\tau) = e^{-(\beta^2+\gamma^2)\tau} \left\langle \frac{1}{a^2} U_{\alpha,11}^{11}(\lambda R) \pi^{-1} sh\pi\beta\lambda^{-(2\alpha+j)} \sum_{j=0}^{2} g_{j0} \times \right.$$

$$\times \left\{ \frac{2^{i\beta-1}\Gamma(i\beta)}{j+\alpha-i\beta} (\lambda R)^{j+\alpha-i\beta} {}_1F_2\left(\frac{j+\alpha-i\beta}{2}; 1-i\beta, \frac{j+\alpha-i\beta+2}{2}; \frac{(\lambda R)^2}{4} \right) + \right.$$

CHAPTER 1

$$+\frac{2^{-i\beta-1}\Gamma(-i\beta)}{j+\alpha+i\beta}(\lambda R)^{j+\alpha+i\beta}{}_1F_2\left(\frac{j+\alpha+i\beta}{2};1+i\beta,\frac{j+\alpha+i\beta+2}{2};\frac{(\lambda R)^2}{4}\right)\Bigg\}-$$

$$-X^{12}_{\alpha 11;}(\lambda R,\beta)\frac{1}{a^2}\lambda^{(j+2\alpha)}\sum_{j=0}^{2}g_{j0}\left\{\frac{(\lambda R)^{j+\alpha+i\beta}}{2^{i\beta}(j+\alpha+i\beta)\Gamma(1+i\beta)}\times\right.$$

$$\left.\times{}_1F_2\left(\frac{j+\alpha+i\beta}{2};\frac{j+\alpha+i\beta+2}{2},1+i\beta;\frac{(\lambda R)^2}{4}\right)\right\}\Bigg\rangle+$$

$$+\frac{sh\pi b}{\pi\lambda^{2\alpha}}\left[\frac{1-e^{-(\beta^2+\gamma^2)\tau}}{(\beta^2+\gamma^2)}a_0+\sum_{n=1}^{\infty}a_n\frac{\left[(\beta^2+\gamma^2)\cos\nu_n^2t+\nu_n^2\sin\nu_n^2t\right]-e^{-(\beta^2+\gamma^2)\tau}(\beta^2+\gamma^2)}{(\beta^2+\gamma^2)^2+(\nu_n^2)^2}\right]. \quad (1.32)$$

Let's apply to the function $\tilde{T}(\tau,\beta)$ the integral operator $H_\alpha^{-1}(\tau,\beta)$.
For non-stationary case:

$$\int_0^\infty e^{-(\beta^2+\gamma^2)t}\frac{sh\pi\beta V_\alpha(r,\beta)\Omega(r,\beta)d\beta}{\pi\lambda^{2\alpha}}g_R=\frac{I_{q,\alpha}(\lambda r)}{U^{11}_{q,\alpha}(\lambda R)}g_R(t),$$

$$\int_0^\infty e^{-(\beta^2+\gamma^2)t}V_\alpha(r,\beta)V_\alpha(\rho,\beta)\Omega(r,\beta)d\beta=\varepsilon(r,\rho,q)=$$

$$=\frac{\lambda^{2\alpha}}{U^{11}_{q,\alpha;11}(\lambda R)}\begin{cases}I_{q,\alpha}(\lambda r)\psi^{1*}_{q,\alpha;11}(\lambda R,\lambda\rho) & 0<r<\rho<R,\\ I_{q,\alpha}(\lambda\rho)\psi^{1*}_{q,\alpha;11}(\lambda R,\lambda r) & 0<\rho<r<R.\end{cases}$$

Numerical analysis. Based on the obtained formulas for determining the temperature at any point of the radius of wooden cylindrical beam at any time of drying depending on the effect of thermal diffusion, initial values of temperature and moisture, thermophysical characteristics of the material and parameters of the drying agent on the temperature of phase transitions, a software program is designed, the work of which is demonstrated for solving a specific application problem of wood drying.

To implement the numerical experiment, the characteristics of the thermophysical properties of wood were used. The dependence of the hydro conductivity of wood on temperature and moisture was derived on the basis of experimental data [6].

Numerical simulation of drying of a sample of a cylindrical pine timber beam of a circular cross-section of the temperature T_0 with a 50 % moisture content was carried out. The following basic parameters of the problem were accepted: ambient temperature T_a, which is determined by the temperature of the steam-air mixture measured by a dry bulb thermometer. The drying process lasted until the temperature of the beam reached the ambient temperature $T_1 = 289$ K. Drying agent velocity $\upsilon = 2$ m/s; saturated vapor density $\rho_v = 0.013188$ kg/m^3; air density $\rho_{a0} = 1.29$ kg/m^3. Physical parameters of wood: the radius of cross-section of a beam $R = 0.25$ m; density 500 kg/m^3; moisture 0.7 kg/kg; porosity $\Pi = 0.672$. Thermal parameters of wood: initial temperature $T_0 = 290$ K, thermal conductivity coefficient $\lambda = 0.14$ W/(m·K).

Computer simulation of the drying of a cylindrical beam was carried out for soft (≈ 300 K) and hard regimes (≈ 370 K), which were determined by the control functions of temperature and moisture of the steam-air mixture, which is fed into the drying chamber.

In **Fig. 1.3** and **1.4**, the temperature distributions in the structural elements of the cylindrical beam are presented. **Fig. 1.3** characterizes the change in temperature in the wooden beam during drying at 300 K; and so, does **Fig. 1.4** at 370 K, respectively.

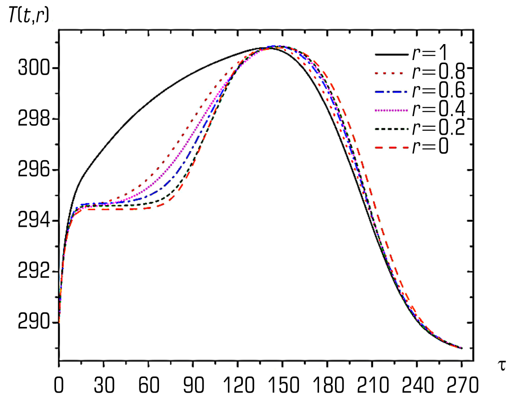

⬡ **Fig. 1.3** Temperature distributions on the surface and inside the cylindrical beam at a drying agent temperature of 302 K (soft regime)

Here, the curve 1 corresponds to a unit value of dimensionless radius $\bar{r} = 1$, i.e., it shows the temperature on the surface of the cylinder; curve 2: $\bar{r} = 0.8$; curve 3: $\bar{r} = 0.6$; curve 4: $\bar{r} = 0.4$; curve 5: $\bar{r} = 0.2$; curve 6 corresponds to zero value of dimensionless radius: $\bar{r} = 0$.

Analyzing the graphical dependences, it is possible to see that in the process of drying cylindrical wood with the specified initial parameters, three characteristic stages are observed: heating, stabilization, and cooling.

The graphical analysis of the drying process for wood with a circular cross-section ($\rho = 500$ kg/m^3) and an initial moisture content 0.7 kg/kg reveals several key insights for both hard and soft drying regimes. Throughout the entire drying process, the temperature of the wood's surface layer is consistently higher than that of the inner layers for both drying regimes. By the end of the first drying period, the surface layer reaches a maximum temperature. The inner layers experience different heating patterns: in the hard drying regime, they experience more rapid temperature increases, indicating quicker heat penetration and more aggressive moisture removal leading to faster vaporization within the wood. In contrast, for the soft drying regime, the bulk of the wood remains within the 294–295 K range for a significant portion of the first period, only beginning to increase in temperature two-thirds of the way through this period. During the second drying period, the temperature growth stabilizes across the layers, attributed to the absorption of heat for internal vaporization. The onset of the constant drying rate period varies with depth, showing significant delays in the wood's inner layers. For hard drying regimes, maximum temperatures are achieved mid-way through this period, followed by a gradual decline. During the period of decreasing drying rate, a noticeable temperature rise occurs throughout the entire material volume until the central layer's temperature matches the surface layer's temperature. This period is dominated by the release of bound moisture, which dictates the duration of the drying process.

It should be noted that the temperature distributions in the cross-sectional layers of wood for the two considered drying regimes differ qualitatively and quantitatively. The temperature of the outer layer of the cylindrical beam during the entire drying period is much higher than the temperature of the middle layers, and, here, the maximum residual pressure is maintained until the end of τ_1. A temperature gradient appears, which causes the flow of moisture to move towards low temperatures, and its place is filled by steam.

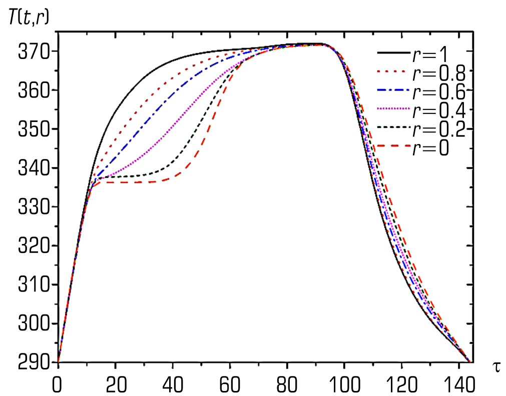

Fig. 1.4 Temperature distributions on the surface and inside the cylindrical beam at a drying agent temperature of 370 K (hard regime)

At hot drying modes during the second period of stabilization we observe a significant difference in the values of the temperature of wood layers in depth, sometimes up to 10 K (**Fig. 1.4**, measurement time 0.5 τ_2, layers $\overline{r}=0.2,\ 0.4,\ 0.6$). Just at this time it is possible to observe the maximum values of internal residual pressures in these layers. In mild regime, an increase in the temperature of the central part of the beam is observed at the time 2/3 τ_2 and a corresponding decrease in moisture content in its core layers (**Fig. 1.3**, time curve 0.7 τ_2). From the third period τ_3, the rate of moisture removal decreases until the state of equilibrium moisture content.

In conclusion, the hard drying regime leads to a quicker internal temperature rise, suggesting faster drying but potentially greater risk of stress and cracking. The soft drying regime offers a gentler approach, with slower internal temperature increases, potentially reducing stress and maintaining structural integrity. This analysis underscores the importance of selecting an appropriate drying regime based on the desired balance between drying speed and material quality preservation.

1.2 SOLVING STEFAN'S LINEAR PROBLEM FOR DRYING CYLINDRICAL BEAM UNDER QUASI-AVERAGED FORMULATION

When solving the problem of drying objects with a capillary-porous structure, in particular wood, they usually are described in terms of a quasi-homogeneous medium [22–25] with effective coefficients, which are chosen so that the solution to the problem in a homogeneous medium would coincide with the solution of the problem in a porous medium. The effect of the porous structure is taken into account by introducing the effective coefficients of binary interaction into the Stefan-Maxwell equation. The problem of mutual distribution of phases is solved according to the principle of local equilibrium of phases [26–31]. The given properties of the material, namely: heat capacity, density, thermal conductivity coefficients are functions of material porosity, density and heat capacity of body components.

The plain problem of drying of a cylindrical timber beam in average statement is considered. The thermal diffusivity coefficients are expressed in terms of the porosity of the timber, the density of the components of vapor, air, and timber skeleton. The problem of mutual phase distribution during drying of timber has been solved using the energy balance equation. The indicators of the drying process of the material depend on the correct choice and observance of the parameters of the drying medium [32].

In stationary mode, the relationship between temperature and moisture gradients is determined by the formula:

$$\frac{\partial U}{\partial r}+\frac{\beta}{a}U=\frac{\delta\,\partial T}{\partial r}-\frac{\beta}{a}U_p,$$

where δ is the thermogradient coefficient; β is the mass transfer coefficient; a is the thermal diffusivity coefficient. In this dependence, the rate of moisture transfer is affected by the rate of heat transfer and by the equilibrium moisture content U_p [19]. The relationship between the distribution of moisture content and temperature fields depends on the geometric dimensions of the timber material in length and radius. Since the length of the beam of material is much larger than the cross-sectional size and the coefficient of moisture conductivity is much larger along the fibers than this coefficient across the fibers and due to the great complexity of the structure of timber material, consider the plane average problem of heat conduction.

When the hot air of the drying agent contacts with the moisture of the dried material, the moisture particles disintegrate and multiply, turning into steam and rarefied moisture particles, the number of which increases [7]. Thus, there is a multiplying of particles of a two-phase zone. At the same time there occurs a gradual deepening of the front of moisture evaporation. Heat is supplied to the evaporation front by heat conduction from the drying agent across the dried layer of material. Excess pressure is formed in the front zone, under the action of which the vapor is filtered to the outer surface. The total rate of moisture removal depends on the thermal and filtration resistance. The vapor pressure and the temperature at the front are related as parameters of saturated vapor. The slow movement of the front into depth allows to consider the fields of temperature and excess pressure in the dried material to be quasi-stationary. The drying process with a variable phase transition boundary is described by the equation [19]:

$$\frac{\partial T}{\partial \tau}+\gamma^2 T=a^2 B_\alpha\left[T,r\right],\ \gamma^2=\frac{\gamma_1^{\ 2}}{C\rho},\ \alpha>0, \tag{1.33}$$

where $a^2=\dfrac{\lambda}{\left[\Pi(C_v\rho_v+C_a\rho_a)+\left(1-\Pi\right)C_s\rho_s\right]}$ is averaged thermal diffusivity coefficient.

Let's solve (1.33) under the initial condition:

$$T\left(\tau,r\right)\Big|_{\tau=0}=g\left(r\right),\ r\in\left(0,R\right), \tag{1.34}$$

and under the boundary conditions on $r=0$ and $r=R$, which express heat exchange in the cylinder and between the surface of the cylinder and the drying agent:

$$\lim\Big|_{r\to 0}\frac{\partial}{\partial r}\left(r^\alpha T\right)=0,\left(\alpha_{11}^1\frac{\partial}{\partial r}+\beta_{11}^1\right)T\Big|_{r\to R}=T_a\left(\tau\right). \tag{1.35}$$

The process of penetration of hot air, the rate of which is proportional to the concentration, leads to the problem of phase transition if $\gamma^2<0$ (diffusion with decomposition), the indices of a series:

$$T\left(M,t\right)=\sum_{n=1}^{\infty}T_n e^{\left(\gamma^2-a^2\lambda\right)t}\upsilon_n\left(M\right),$$

obtained by expansion in terms of eigenvalues functions $\upsilon_n(M)$, are less than the indices of a series if not to take into account changes in temperature over time without a phase transition. In the case $\gamma^2 > 0$ (penetration with multiplication), if at least one of the indices $(\gamma^2 - a^2\lambda) > 0$, then there is an increase by the exponential law. The value γ^2 is a characteristics of the material (multiplication factor), λ significantly depends on the shape and size of the area (pores). If $\lambda = \frac{\gamma^2}{a^2}$, then the area where the phase transition occurs has critical dimensions. For a plane problem, the smallest value of λ corresponds to the eigenfunction, which has radial symmetry and is equal to $\lambda_1 = \frac{\mu_1^{(0)}}{R}$, $\mu_1^{(0)} = 2.4048$ [19].

For the critical diameter, the formula $d_{kp} = \frac{2\mu_1^{(0)}a}{\gamma} = \frac{4.80a}{\gamma}$ is obtained [29].

When solving the problem of drying objects with a capillary-porous structure, in particular wood, in order not to consider the porous body in all its complexity, it is described in terms of a quasi-homogeneous medium with effective coefficients, which are chosen so that the solution of the problem in a homogeneous medium coincides with the solution in a porous medium. The influence of the porous structure is taken into account by introducing the effective binary interaction coefficients into the Stefan-Maxwell equation. The problem of mutual phase distribution is solved using the principle of local phase equilibrium. It is possible to consider that the averaged properties of the material, namely: heat capacity C, density ρ, and thermal conductivity coefficients λ are functions of porosity of material, densities and heat capacities of body components.

Problem statement. Let's consider the problem of drying a wet long wooden beam of cylindrical cross section in a drying plant. In solving this problem, it is possible to neglect the discrete structure of the material at the molecular level and come to the equation of heat conduction:

$$\frac{\partial T}{\partial \tau}(\rho, \tau) = a\Delta T + \gamma^2 T,\ \gamma^2 > 0.$$

Here, a is the thermal diffusivity coefficient, γ is a variable equivalent to the presence of sources of diffusing substance in the pores, T is the body temperature. The higher the temperature is the higher the rate of drying. The temperature in the drying chamber is the temperature in the vapor-gas mixture, which is determined by a dry bulb thermometer. The temperature determined by a wet bulb thermometer is the temperature at the boundary of the phase transition, which moves inside the material. The difference between the readings of dry and wet bulb thermometers is used to determine the relative humidity. For successful air drying, a continuous flow of air throughout the beam must be ensured. In the drying chambers, unsaturated air is used as a drying agent. Successful operation of drying chambers is achieved by regulating the temperature and humidity at the right time [33–37].

The volume of the dried area is a function of time. In the this case, the body to be dried is a cylindrical beam, the outer surface of which $F(r,\tau) = 0$ is described by the equation:

$$F(r,\tau) = r - 1 = 0,\ \tau = 0. \tag{1.36}$$

At the time moment $\tau = 0$, the temperature $T_0(\tau)$ is applied to the outer surface of the cylinder and from this time the drying process begins, and at the interface of the phase transition the curve of separation of dry and wet zones is the temperature $T_c(\tau)$ curve.

In the process of drying, this curve moves, forming a closed curve $F_k(r,\tau) = 0$, which is an isotherm $T = T_c$. In the zone where the drying has already taken place, the temperature is described by the equation of heat conduction and by boundary conditions, these boundary conditions can be written as:

– on the outer contour of the cylinder $F_k(r,\tau) = 0$:

$$T = T_c, \tag{1.37}$$

– and the following initial conditions:

$$T = T_0,\ F_0 = F_k,\ \tau = 0. \tag{1.38}$$

Let $V(F_k, F_0)$ be the volume of the dried area at the time t per unit length of the beam in the direction of the axis Oz. Then, over a period of time Δt, the volume will increase by $\Delta V(F_k, F_0)$, and the amount of heat spent is:

$$\Delta Q = \rho_k c_k \left(T - T_c\right) \Delta V\left(F_k, F_0\right). \tag{1.39}$$

Determine this amount of heat through the flow on the surface $F_k(r,\tau) = 0$:

$$\Delta Q = -\lambda_k \int_{F_k l=0} \frac{\partial T}{\partial n} ds \Delta t. \tag{1.40}$$

Passing in (1.40) to the limit at $\Delta t \to 0$, given (1.39), let's obtain:

$$\lambda_k \int_{F_k l=0} \frac{\partial T}{\partial n} ds = -\rho_k c_k \left(T - T_c\right) \frac{dV\left(F_k, F_0\right)}{dt}, \tag{1.41}$$

$$V\left(F_k, F_0\right) = \int \int_{F_k=0}^{F_0=0} ds. \tag{1.42}$$

If to pass to the variables:

$$\eta = \frac{T - T_c}{T_0 - T_c},\ \beta = \frac{\rho_k c_k a}{\lambda_k},\ \vartheta = \frac{V}{R^2},\ l = \frac{s}{R},\ \sigma = \frac{s}{R^2}, \tag{1.43}$$

then dimensionless coefficients will satisfy the equation of heat conduction and the boundary conditions (1.37), (1.38):

at $F_0 = 0$,

$\eta = 1$;

at $F_k = 0$,

$$\eta = 0; \tag{1.44}$$

$$\eta = 1,\ \tau = 0. \tag{1.45}$$

Let's consider the equation of the Stefan's boundary change:

$$\beta\eta \frac{d\vartheta}{d\tau} = -\frac{\partial T}{\partial n} dl, \tag{1.46}$$

$$\vartheta\left(F_0, F_k\right) = \int \int_{F_k = 0}^{F_0 = 0} d\sigma. \tag{1.47}$$

It is possible to note that at the beginning of the drying process:

$$F_k\left(x, y, \tau\right) = F_0\left(x, y\right),\ \varepsilon^*\left(t\right) = 0. \tag{1.48}$$

Over a short period of time, the contour of the boundary of the dried and wet zones will be as follows:

$$F_k\left(x, y, t\right) - F_0\left(x_1, y_1\right) = \varepsilon^*\left(t\right), \tag{1.49}$$

where $\varepsilon^*(t)$ is the thickness of the layer of the dried area (1.49). From the symmetry of the problem it follows that the contours F_0, F_k are concentric circles, the equations of which in a dimensionless polar system are:

$$F_0 = r - 1 = 0,\ F_k(t) = r - 1 + \varepsilon(t) = 0,\ \varepsilon = \frac{\varepsilon^*}{R}. \tag{1.50}$$

With this $\varepsilon(\tau) = 0$ for $\tau = 0$.

From (1.50) it follows that at the time of complete drying of the beam $\varepsilon^*(t) = R$, and, respectively, $\varepsilon(\tau) = 1$.

Write the equation of heat balance for the area bounded by the contours F_0, $F_k(t)$. In integral form, this equation can be written as:

$$\int \int_{F_k=0}^{F_0=0} \frac{\partial\eta}{\partial\tau} d\sigma = \int_{F_0 l} \frac{\partial\eta}{\partial n} dl - \int_{F_{kl}} \frac{\partial\eta}{\partial n} dl, \tag{1.51}$$

where F_{0l}, F_{kl} are contours of cross-sections of surfaces $F_0 = 0$, $F_k = 0$, respectively.

If to take into account the boundary condition (1.46), it is possible to obtain:

$$\int \int_{F_k=0}^{F_0=0} \frac{\partial\eta}{\partial n} d\sigma = \int_{F_{0k}} \frac{\partial\eta}{\partial n} dl + \beta\eta \frac{\partial\eta}{\partial\tau}. \tag{1.52}$$

Equation (1.52) is the main one, which takes into account the factor of the moving boundary.

Introduce the function $\eta^*(r,\tau)$ so that it satisfies the initial and boundary conditions (1.45). This function will establish the relationship between the relative saturation and temperature in the cross section in time.

$$\eta^*(r,\tau) = \frac{r - 1 + \varepsilon(\tau)}{\varepsilon(\tau)}. \tag{1.53}$$

Let's take $\eta^*(r,\tau)$ as an approximate solution, which at a certain value $\varepsilon(\tau)$ must satisfy (1.51). There is a relationship between it and ε:

$$\frac{\partial\eta^*}{\partial\tau} = (1 - r)\frac{1}{\varepsilon^2}\frac{d\varepsilon}{dt},\ \frac{\partial\eta^*}{\partial n} = \frac{\partial\eta^*}{\partial r} = \frac{1}{\varepsilon}, \tag{1.54}$$

$$\int_{F_{0l}} \frac{\partial\eta^*}{\partial n} dl = \frac{2\pi}{\varepsilon},\ \int \int_{F_k=0}^{F_0=0} \frac{\partial\eta^*}{\partial n} d\sigma = \int_0^{2\pi} d\varphi \int_{1-\varepsilon}^{1} \frac{1-r}{\varepsilon^2}\frac{d\varepsilon}{d\tau} r dr = \frac{\pi}{3}(3 - 2\eta)\frac{d\varepsilon}{d\tau}.$$

From (1.52) it is possible to obtain:

$$\varepsilon^2 + \varepsilon \frac{1 - 2\beta\eta^*}{2(3\beta\eta^* - 1)} \frac{d\varepsilon}{d\tau} = \frac{3\beta\eta^*}{3\beta\eta^* - 1}, \tag{1.55}$$

or

$$d\tau = \frac{1}{B}\left(\varepsilon^2 + A\varepsilon\right)d\varepsilon,\ \tau(0) = 0, \tag{1.56}$$

$$B = \frac{3\beta\eta^*}{3\beta\eta^* - 1},\ A = \frac{1 - 2\beta\eta *}{2(3\beta\eta * -1)}. \tag{1.57}$$

The solution of (1.56) is:

$$\tau = \frac{1}{B}\left(\frac{\varepsilon^3}{3} + A\frac{\varepsilon^2}{2}\right). \tag{1.58}$$

From (1.46) and (1.58), taking into account (1.47) and (1.50), it is possible to obtain the equation describing the change in the unit of length of the volume of the dried zone over time: $V_d = \pi R^2\left[1 - \varepsilon^2(\tau)\right]$ and, thus, now it is possible to calculate the relative moisture of the timber beam during drying $W = \frac{V - V_d}{V}$. Simple formulae for approximation of the experimental data allow to calculate the total duration of the drying process from the initial to the final moisture content of the material.

Numerical experiment. Based on the obtained solutions, the numerical simulation of drying of samples of timber circular beams of pine, spruce, and birch of the same size has been carried out. The material after preliminary natural drying had been brought to 15 % of moisture content. The following basic parameters of the problem have been accepted: the ambient temperature T_c = 313 K; the velocity of the drying agent υ = 2m/s; the saturated vapor density ρ_n = 0.013188 kg/m^3; the air density ρ_{a0} = 1.29 kg/m^3. Physical parameters of timber: the radius of a circular beam R = 0,07 m; wood density: spruce 450 kg/m^3, pine 500 kg/m^3, birch 750 kg/m^3; the porosity: pine Π = 0.672, spruce Π = 0.654, birch Π = 0.591. Thermal parameters of wood: the initial temperature T_0 = 293 K, the thermal conductivity coefficient at moisture of 15 % across fibers: spruce λ = 0.11 W/(m·K), pine λ = 0.14 W/(m·K), birch λ = 0.14 W/(m·K).

Fig. 1.5 shows the changes in the thickness of the layer of the dried area ε in time of drying τ.

In **Fig. 1.6**, the distributions of relative moisture of wood in time are presented.

The analysis of the relative moisture content for different species of wood: spruce, pine, and birch, during the drying process reveals distinct drying dynamics for each wood type.

It is possible to observe that the samples with greater porosity and lower density lose moisture faster (**Fig. 1.6**, curves 1, 2); the moisture from wood with less porosity is removed more slowly (**Fig. 1.6**, curve 3). The obtained results correspond to the experimental data given in the literature [38–40].

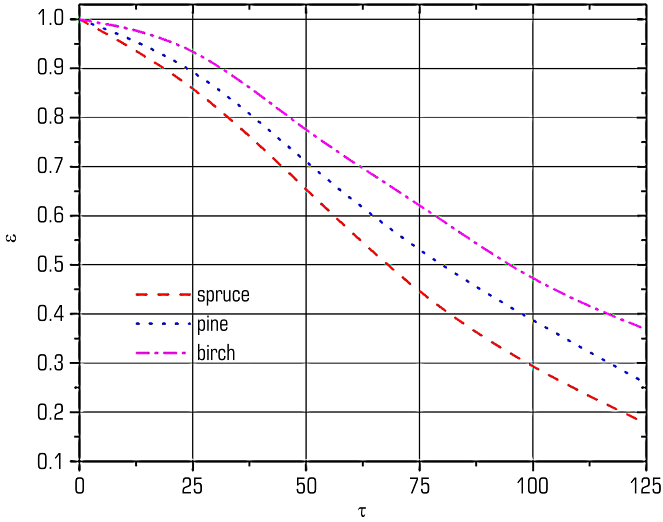

Fig. 1.5 The dependence of thickness of layer of the dried area on time of drying (curves 1–3 correspond to sort of materials: spruce, pine, birch, respectively)

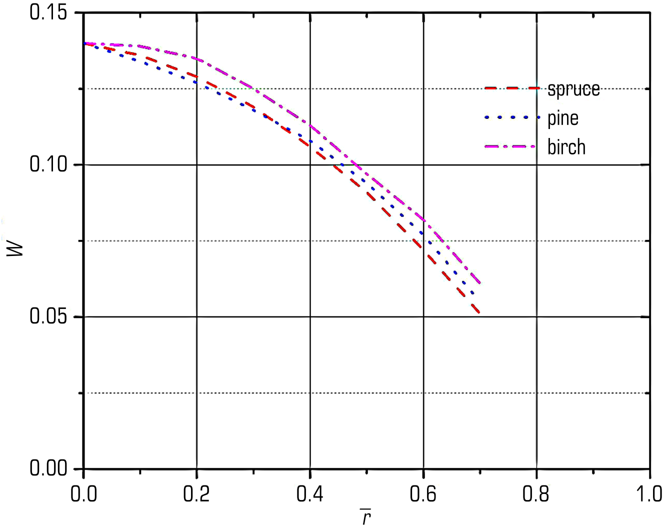

Fig. 1.6 Change in relative moisture of beam skeleton in time (curves 1–3 correspond to materials: spruce, pine, birch, respectively)

CONCLUSIONS

The two problems of convective drying of wood of the circular cross-section in nonstationary and quasi-stationary formulations have been solved taking into account given properties of the material: heat capacity, density, thermal diffusivity coefficients, which are expressed as functions of the porosity of the material, densities, and heat capacities of the components.

In the first problem, a nonlinear mathematical model for forecasting the drying behavior of cylindrical beams of capillary-porous material under convective conditions is constructed, enabling more accurate control and optimization of the drying process in industrial applications. The governing equations for heat transfer are formulated, which are discretized using finite difference approximations for derivatives. The Kontorovich-Lebedev transform is used to simplify the complex differential equations that arise due to the cylindrical symmetry of the wood. Green's functions are employed to address the inhomogeneous differential equations representing the system's response to initial and boundary conditions. Analytical dependences are obtained for determining the temperature based on the thermophysical characteristics of the material and the parameters of the drying agent in non-isothermal conditions. The solution to Bessel equations involved Bessel functions of the first and the second kinds, which were computed using their series expansions as well as numerical libraries of special functions in Python. When approximating series solutions, Pochhammer's polynomials are utilized, making it easier to capture the behaviors of heat distribution in the wood profile. Steklov's theorem ensures that the series solutions used in the model are convergent and orthogonal. The resulting system of algebraic equations is solved iteratively to obtain the temperature distributions within the wood. Boundary conditions are applied to simulate real drying conditions, ensuring that the model accurately reflects the physical processes involved.

For the second problem about mutual phase distribution, the relationship is established between the drying time and the average parameters of porous cylindrical timber, in particular the relative saturation of moisture, the thermal conductivity of timber, which take into account the factor of movement of the transient boundary of the dried zone. It has been established that in the process of drying timber materials, the movable surface of the phase transition, which separates the dried and wet zones, depends on the properties of the material and temperature, which is a function of coordinates and time. The results are in good agreement with experimental data and results of other research.

The study bridges the gap between theoretical models and practical applications by providing a robust framework that accommodates the complex interactions involved in wood drying.

REFERENCES

1. Burak, Ya. Y., Chaplia, Ye. Ya., Chernukha, O. Yu. (2006). Kontynualno-termodynamichni modeli mekhaniky tverdykh rozchyniv. Kyiv: Naukova dumka, 272.

2. Sokolovskyy, Y., Levkovych, M., Mysyk, M. (2023). Matrix Approach to Numerical Modeling of Heat-and-Moisture Transfer Processes in a Medium with a Fractal Structure. 2023 17th International Conference on the Experience of Designing and Application of CAD Systems (CADSM), 44–48. https://doi.org/10.1109/cadsm58174.2023.10076519
3. Lykov, A. V. (1968). Teoriia sushki. Moscow: Energiia, 472.
4. Hachkevych, O. R., Kushnir, R. M., Terletskii, R. F. (2022). Mathematical Problems of Thermomechanics for Deformable Bodies Subjected to Thermal Irradiation. Ukrainian Mathematical Journal, 73 (10), 1522–1536. https://doi.org/10.1007/s11253-022-02011-7
5. Kheifitc, L. I., Neimark, A. V. (1982). Mnogofaznye protcessy v poristykh sredakh. Moscow: Khimiia, 320.
6. Pyanylo, Y. (2022). Analysis of Filtration Processes in Porous Environments Taking Into Aaccount the Movement of Capillaries. 2022 12th International Conference on Advanced Computer Information Technologies (ACIT), 9–12. https://doi.org/10.1109/acit54803.2022.9913087
7. Gayvas, B., Markovych, B., Dmytruk, A., Havran, M., Dmytruk, V. (2024). The methods of optimization and regulation of the convective drying process of materials in drying installations. Mathematical Modeling and Computing, 11 (2), 546–554. https://doi.org/10.23939/mmc2024.02.546
8. Hayvas, B., Dmytruk, V., Torskyy, A., Dmytruk, A. (2017). On methods of mathematical modeling of drying dispersed materials. Mathematical Modeling and Computing, 4 (2), 139–147. https://doi.org/10.23939/mmc2017.02.139
9. Baranovsky, S. V., Bomba, A. Ya. (2024). The diffusion scattering parameters identification for a modified model of viral infection in the conditions of logistic dynamics of immunological cells. Mathematical Modeling and Computing, 11 (1), 59–69. https://doi.org/10.23939/mmc2024.01.059
10. Mozhaev, A. P. (2001). Chaotic homogeneous porous media. 1. Theorems about structure. Engineering-Physical Journal, 74 (5), 196–201.
11. Lutcyk, P. P. (1988). Issledovanie protcessov teplomassoperenosa pri sushke kapilliarno-poristykh tel s uchetom vnutrennikh napriazhenii. Teplomassoobmen. Minsk: Institut teplo- i massoobmena im. A. V. Lykova, 184–197.
12. Khoroshun, L. P., Maslov, B. P., Leshchenko, P. V. (1989). Prognozirovanie effektivnykh svoistv pezoaktivnykh kompozitcionnykh materialov. Kyiv: Naukova dumka, 208.
13. Burak, Y., Kondrat, V., Gayvas, B. (2002). On the mathematical modeling of drying processes of porous bodies. Informational-Mathematical Modeling of Complex Systems. Lviv: CMM IPPMM named after Y. S. Pidstryhach NAS of Ukraine, Akhil Publishing House, 153–159.
14. Dibagar, N., Kowalski, S. J., Chayjan, R. A., Figiel, A. (2020). Accelerated convective drying of sunflower seeds by high-power ultrasound: Experimental assessment and optimization approach. Food and Bioproducts Processing, 123, 42–59. https://doi.org/10.1016/j.fbp.2020.05.014

15. Shlikhting, G. (1974). Teoriia pogranichnogo sloia. Moscow: Nauka, 690.
16. Gayvas, B. I., Dmytruk, V. A., Semerak, M. M., Rymar, T. I. (2021). Solving Stefan's linear problem for drying cylindrical timber under quasi-averaged formulation. Mathematical Modeling and Computing, 8 (2), 150–156. https://doi.org/10.23939/mmc2021.02.150
17. Gayvas, B. I., Dmytruk, V. A. (2022). Investigation of drying the porous wood of a cylindrical shape. Mathematical Modeling and Computing, 9 (2), 399–415. https://doi.org/10.23939/mmc2022.02.399
18. Gayvas, B. I., Markovych, B. M., Dmytruk, A. A., Havran, M. V., Dmytruk, V. A. (2023). Numerical modeling of heat and mass transfer processes in a capillary-porous body during contact drying. Mathematical Modeling and Computing, 10 (2), 387–399. https://doi.org/10.23939/mmc2023.02.387
19. Gera, B., Kovalchuk, V., Dmytruk, V. (2022). Temperature field of metal structures of transport facilities with a thin protective coating. Mathematical Modeling and Computing, 9 (4), 950–958. https://doi.org/10.23939/mmc2022.04.950
20. Gayvas, B., Markovych, B., Dmytruk, A., Dmytruk, V., Kushka, B., Senkovych, O. (2023). Study of Contact Drying Granular Materials in Fluidized Bed Dryers. 2023 IEEE XXVIII International Seminar/Workshop on Direct and Inverse Problems of Electromagnetic and Acoustic Wave Theory (DIPED), 238–241. https://doi.org/10.1109/diped59408.2023.10269464
21. Alaa, K., Atounti, M., Zirhem, M. (2021). Image restoration and contrast enhancement based on a nonlinear reaction-diffusion mathematical model and divide & conquer technique. Mathematical Modeling and Computing, 8 (3), 549–559. https://doi.org/10.23939/mmc2021.03.549
22. Alaa, H., Alaa, N. E., Aqel, F., Lefraich, H. (2022). A new Lattice Boltzmann method for a Gray–Scott based model applied to image restoration and contrast enhancement. Mathematical Modeling and Computing, 9 (2), 187–202. https://doi.org/10.23939/mmc2022.02.187
23. Baala, Y., Agmour, I., Rachik, M. (2022). Optimal control of tritrophic reaction–diffusion system with a spatiotemporal model. Mathematical Modeling and Computing, 9 (3), 647–662. https://doi.org/10.23939/mmc2022.03.647
24. Bounkaicha, C., Allali, K., Tabit, Y., Danane, J. (2023). Global dynamic of spatio-temporal fractional order SEIR model. Mathematical Modeling and Computing, 10 (2), 299–310. https://doi.org/10.23939/mmc2023.02.299
25. Gouasnouane, O., Moussaid, N., Boujena, S., Kabli, K. (2022). A nonlinear fractional partial differential equation for image inpainting. Mathematical Modeling and Computing, 9 (3), 536–546. https://doi.org/10.23939/mmc2022.03.536
26. Najm, F., Yafia, R., Aziz Alaoui, M. A., Aghriche, A., Moussaoui, A. (2023). A survey on constructing Lyapunov functions for reaction-diffusion systems with delay and their application in biology. Mathematical Modeling and Computing, 10 (3), 965–975. https://doi.org/10.23939/mmc2023.03.965

27. Suganya, G., Senthamarai, R. (2022). Mathematical modeling and analysis of Phytoplankton–Zooplankton–Nanoparticle dynamics. Mathematical Modeling and Computing, 9 (2), 333–341. https://doi.org/10.23939/mmc2022.02.333
28. Ben-Loghfyry, A., Hakim, A. (2022). Time-fractional diffusion equation for signal and image smoothing. Mathematical Modeling and Computing, 9 (2), 351–364. https://doi.org/10.23939/mmc2022.02.351
29. Kostrobij, P. P., Markovych, B. M., Ryzha, I. A., Tokarchuk, M. V. (2021). Statistical theory of catalytic hydrogen oxidation processes. Basic equations. Mathematical Modeling and Computing, 8 (2), 267–281. https://doi.org/10.23939/mmc2021.02.267
30. Kostrobij, P. P., Ivashchyshyn, F. O., Markovych, B. M., Tokarchuk, M. V. (2021). Microscopic theory of the influence of dipole superparamagnetics (Type $\langle\beta$–CD$\langle$FeSO4$\rangle\rangle$) on current flow in semiconductor layered structures (type gase, inse). Mathematical Modeling and Computing, 8 (1), 89–105. https://doi.org/10.23939/mmc2021.01.089
31. Aberqi, A., Elmassoudi, M., Hammoumi, M. (2021). Discrete solution for the nonlinear parabolic equations with diffusion terms in Museilak-spaces. Mathematical Modeling and Computing, 8 (4), 584–600. https://doi.org/10.23939/mmc2021.04.584
32. Bazirha, Z., Azrar, L. (2024). DDFV scheme for nonlinear parabolic reaction-diffusion problems on general meshes. Mathematical Modeling and Computing, 11 (1), 96–108. https://doi.org/10.23939/mmc2024.01.096
33. Baranovsky, S., Bomba, A., Lyashko, S., Pryshchepa, O. (2024). Diffusion Perturbations in Models of the Dynamics of Infectious Diseases Taking into Account the Concentrated Effects. Computational Methods and Mathematical Modeling in Cyberphysics and Engineering Applications 1, 273–303. https://doi.org/10.1002/9781394284344.ch11
34. El Hassani, A., Bettioui, B., Hattaf, K., Achtaich, N. (2024). Global dynamics of a diffusive SARS-CoV-2 model with antiviral treatment and fractional Laplacian operator. Mathematical Modeling and Computing, 11 (1), 319–332. https://doi.org/10.23939/mmc2024.01.319
35. Tokarchuk, M. V. (2023). Unification of kinetic and hydrodynamic approaches in the theory of dense gases and liquids far from equilibrium. Mathematical Modeling and Computing, 10 (2), 272–287. https://doi.org/10.23939/mmc2023.02.272
36. Belhachmi, Z., Mghazli, Z., Ouchtout, S. (2022). A coupled compressible two-phase flow with the biological dynamics modeling the anaerobic biodegradation process of waste in a landfill. Mathematical Modeling and Computing, 9 (3), 483–500. https://doi.org/10.23939/mmc2022.03.483
37. Pukach, P. Y., Chernukha, Y. A. (2024). Mathematical modeling of impurity diffusion process under given statistics of a point mass sources system. I. Mathematical Modeling and Computing, 11 (2), 385–393. https://doi.org/10.23939/mmc2024.02.385
38. Laham, M. F., Ibrahim, S. N. I. (2023). Penalty method for pricing American-style Asian option with jumps diffusion process. Mathematical Modeling and Computing, 10 (4), 1215–1221. https://doi.org/10.23939/mmc2023.04.1215

39. Dmytryshyn, L. I., Dmytryshyn, M. I., Olejnik, A. (2023). Model of money income diffusion in the European integration context. Mathematical Modeling and Computing, 10 (2), 583–592. https://doi.org/10.23939/mmc2023.02.583
40. Patil, J. V., Vaze, A. N., Sharma, L., Bachhav, A. (2021). Study of calcium profile in neuronal cells with respect to temperature and influx due to potential activity. Mathematical Modeling and Computing, 8 (2), 241–252. https://doi.org/10.23939/mmc2021.02.241